


December 2014

# Oligomerization of the Sterile-2 G-Protein Coupled Receptor in Yeast Cells in the Presence and Absence of Alpha-Factor Pheromone Using Fluorescence Spectroscopy and Forster Resonance Energy Transfer Analysis

Joel David Paprocki

*University of Wisconsin-Milwaukee*

Follow this and additional works at: <https://dc.uwm.edu/etd>

 Part of the [Biology Commons](#), [Biophysics Commons](#), and the [Physics Commons](#)

---

## Recommended Citation

Paprocki, Joel David, "Oligomerization of the Sterile-2 G-Protein Coupled Receptor in Yeast Cells in the Presence and Absence of Alpha-Factor Pheromone Using Fluorescence Spectroscopy and Forster Resonance Energy Transfer Analysis" (2014). *Theses and Dissertations*. 745.

<https://dc.uwm.edu/etd/745>

This Thesis is brought to you for free and open access by UWM Digital Commons. It has been accepted for inclusion in Theses and Dissertations by an authorized administrator of UWM Digital Commons. For more information, please contact [open-access@uwm.edu](mailto:open-access@uwm.edu).

OLIGOMERIZATION OF THE STERILE-2 G-PROTEIN COUPLED RECEPTOR IN  
YEAST CELLS IN THE PRESENCE AND ABSENCE OF  $\alpha$ -FACTOR PHEROMONE  
USING FLUORESCENCE SPECTROSCOPY AND FÖRSTER RESONANCE ENERGY  
TRANSFER ANALYSIS

by

Joel David Paprocki

A Thesis Submitted in  
Partial Fulfillment of the  
Requirements for the Degree of

Master of Science  
in Physics

at

The University of Wisconsin-Milwaukee

December 2014

## ABSTRACT

OLIGOMERIZATION OF THE STERILE-2 G-PROTEIN COUPLED RECEPTOR IN YEAST CELLS IN THE PRESENCE AND ABSENCE OF  $\alpha$ -FACTOR PHEROMONE USING FLUORESCENCE SPECTROSCOPY AND FÖRSTER RESONANCE ENERGY TRANSFER ANALYSIS

by

Joel David Paprocki

The University of Wisconsin-Milwaukee, 2014  
Under the Supervision of Professor Valerică Raicu

G-protein-coupled receptors (GPCRs) are the largest family of receptors that respond to a wide variety of extracellular stimuli, including molecular ligands such as odorants, neurotransmitters, and hormones, as well as physical agents such as light and pressure. The stimulation event results in initiating conformational changes in the structure of the receptor, which further results in the release of the heterotrimeric G-protein; the latter has a variety of functions within signaling pathways in cellular biology. The GPCR explored in this investigation is the Sterile 2  $\alpha$ -factor receptor (Ste2), whose natural function is that of a yeast mating pheromone receptor. Its natural ligand is the  $\alpha$ -factor mating pheromone, and was used to study the interaction of dynamic hetero-oligomers of Ste2 receptors in the presence and absence of the ligand. Förster Resonance Energy Transfer (FRET), a non-radiative process of energy transfer between fluorescent molecules, was used to probe interactions between protomers within homo-oligomers of Ste2 in living *Saccharomyces cerevisiae* (yeast) cells and hence the general association stoichiometry and quaternary structure. Through the use of spectrally-resolved two-photon microscopy with pixel-level resolution, the interaction between differently fluorescent tagged proteins was explored by determining their apparent FRET efficiency at each pixel. It

was found that Ste2 forms both dimers and tetramers, and with the introduction of its natural ligand, the equilibrium might be shifted from dimers to tetramers.

# TABLE OF CONTENTS

|  |          |
|--|----------|
| Cover Page   |          |
| Abstract   | ii-iii   |
| Table of Contents  | iv       |
| List of Figures  | v        |
| List of Tables   | vi       |
| List of Abbreviations  | vii-viii |
| Acknowledgements   | ix       |
| 1. Introduction  |          |
| 1.1. History and Background  | 1-3      |
| 1.2. Literature Review on a Model GPCR: The Yeast Pheromone Receptor   | 3-6      |
| 1.3. Förster Resonance Energy Transfer   | 6-8      |
| 2. Materials and Methods   |          |
| 2.1. Sample Preparation  |          |
| 2.1.1. Genetic Constructs  | 9        |
| 2.1.2. Cell Growth   | 10-11    |
| 2.1.3. Adherence and Immobilization of Yeast Cells for Imaging   | 11-12    |
| 2.2. Two-Photon Fluorescence Micro-Spectroscopy  | 13-14    |
| 2.3. Choosing the FRET Pairs   | 14       |
| 2.4. Emission Spectra  | 14-15    |
| 2.5. Unmixing of Measured Fluorescence Spectra   | 15-17    |
| 2.6. Signal Unmixing Details and Method  |          |
| 2.6.1. Threshold Based on Signal to Noise Ratio  | 17-18    |
| 2.6.2. Fluorescence Background Subtraction   | 18       |
| 2.6.3. Theory of the Method  | 18-21    |
| 2.7. Determination of Donor and Acceptor Concentrations  | 21-29    |
| 3. Theoretical Modelling   |          |
| 3.1. Analysis of $E_{app}$ Histograms  | 30-32    |
| 3.2. Development of the Dimer and Tetramer Model   |          |
| 3.2.1. Theoretical Modeling of the $E_{app}$ Histograms in Terms of the Dimer Model  | 32-36    |
| 3.2.2. Probability of Donors and Acceptors, and Calculating $E_{app}$ from Dimer Mixing  | 36-38    |
| 3.2.3. Theoretical Modeling of FRET Efficiencies in the Parallelogram-Shaped Tetramer  | 38-41    |
| 4. Results and Discussion  |          |
| 4.1. Refining the Quaternary Structure of Ste2   |          |
| 4.1.1. Determination of the Smallest Oligomer Size   | 42-47    |
| 4.1.2. Probing for Higher Order Oligomers  | 47-52    |
| 4.1.3. Distribution of Apparent FRET Efficiencies  | 52-53    |
| 4.2. Accessing the Effect of Ligand on Populations of Dimers and Tetramers   |          |
| 4.2.1. Determination of Concentrations of Ste2 Receptors in Living Cells Through Calibration via Protein Solution Measurements | 53-57    |
| 4.2.2. FRET Efficiency vs. Concentration of Ste2 Receptors in the Presence and Absence of Ligand                               | 57-61    |
| 5. Conclusions and Future Directions   | 62-64    |
| References   | 65-67    |

## LIST OF FIGURES

|   |    |
|---|----|
| 1. Figure 1.1: Schematic of yeast mating process  | 4  |
| 2. Figure 3.2: Parallelogram-shaped tetramer geometry, and the variables used to theoretically fit a histogram or meta-histogram  | 39 |
| 3. Figure 4.1: Images obtained experimentally, and their resultant $E_{app}$ map and FRET efficiency histogram  | 43 |
| 4. Figure 4.2: Example configurations of dimers, tetramers, and dimer + tetramers that yield a variety of fractions of $E_p$  | 45 |
| 5. Figure 4.3: Meta-histograms of experimental data fit with the dimer model in the absence and presence of ligand  | 46 |
| 6. Figure 4.4: Meta-histograms of experimental data for cells in various ranges of $F^D$ only compared with the total number of cells in the absence and presence of ligand | 47 |
| 7. Figure 4.5: Sampling of histograms of cells at every expression level showing measureable peaks beyond $E_d$   | 50 |
| 8. Figure 4.6: Histograms of cells with only low $F^D$ only values fit with the parallelogram tetramer model  | 52 |
| 9. Figure 4.7: Slope calculation of measured donor (GFP <sub>2</sub> ) protein solutions  | 56 |
| 10. Figure 4.8: Slope calculation of measured acceptor (YFP) protein solutions  | 57 |
| 11. Figure 4.9: Plots of average $E_{app}$ vs. $X_A$ for various ranges of total concentration of donors and acceptors  | 60 |

## LIST OF TABLES

1. Table 3.1:  $E_{app}$  Peaks Predicted by the Parallelogram Tetramer Model according to their configuration of the protomers 40-41

## LIST OF ABBREVIATIONS

1. FRET: Förster Resonance Energy Transfer
2. RET: Resonance energy transfer
3. Ste2 or Ste2p: Sterile-2 Alpha Factor Pheromone Receptor Protein
4.  $E_{app}$ : Apparent FRET Efficiency
5.  $F^D$ : Donor Only Fluorescent Intensity
6.  $E_d$ : Pairwise FRET Efficiency attributed to a dimer constructed from a single donor and acceptor
7.  $E_p$ : Pairwise FRET Efficiency attributed to a tetramer
8.  $Q^A$ : Quantum Yield of the Acceptor
9.  $Q^D$ : Quantum Yield of the Donor
10. G-protein: Guanine nucleotide-binding protein
11. GPCR: G-protein-coupled receptor
12. FRAP: Fluorescence Recovery After Photobleaching
13. CLEM: Correlative Light and Electron Microscopy
14. d-opioid receptor: Delta opioid receptor
15. kDa: kilo-Dalton
16. FCS: Fluorescence Correlation Spectroscopy
17. SpiDA: Spatial Intensity Distribution Analysis
18. D: Donor
19. A: Acceptor
20. GFP<sub>2</sub>: Green Fluorescent Protein, modified version 2
21. YFP: Yellow Fluorescent Protein
22. nm: nanometer
23.  $\mu$ L: microliter
24. mL: milliliter
25. mg: milligram
26. KCl: Potassium Chloride
27. mM: millimolar
28.  $\mu$ M: micromolar
29. Con A: Concanavalin A
30. NA: Numerical Aperture
31. mW: milliwatt
32. 2D: Two-Dimensional
33. EMCCD: Electron-multiplying charged-coupled device
34. CCD: Charged-coupled device
35. OptiMiS: Optical Microscopy System
36. OptiMiS DC: Optical Microscopy System Data-Cruncher
37.  $\mu$ s: microseconds
38. mm: millimeter
39. W: Watt



40.  $w^A$ : Spectral integral of the acceptor
41.  $w^D$ : Spectral integral of the donor
42.  $F^D$  (FRET): Donor only emission in the presence of FRET
43.  $F^A$  (FRET): Acceptor only emission in the presence of FRET
44.  $k^{DA}$  and  $F^{DA}$ : Fluorescence emission from the donor in the presence of an acceptor
45.  $k^{AD}$  and  $F^{AD}$ : Fluorescence emission from the acceptor in the presence of a donor
46.  $\lambda_{ex}$ : Excitation wavelength
47.  $\lambda_{em}$ : Emission wavelength
48.  $\lambda_1$ : Excitation wavelength one
49.  $\lambda_2$ : Excitation wavelength two
50.  $i^D$ : Normalized emission intensities of the donors
51.  $i^A$ : Normalized emission intensities of the acceptors
52.  $\Gamma^{\lambda_1, D}$ : Rate of de-excitation of the donor at the first excitation wavelength
53.  $\Gamma^{\lambda_2, D}$ : Rate of de-excitation of the donor at the second excitation wavelength
54.  $\Gamma^{\lambda_1, A}$ : Rate of de-excitation of the acceptor at the first excitation wavelength
55.  $\Gamma^{\lambda_2, A}$ : Rate of de-excitation of the acceptor at the second excitation wavelength
56.  $\Gamma^{r, D}$ : rate constants of de-excitation through radiative processes of the donor
57.  $\Gamma^{nr, D}$ : rate constants of de-excitation through non-radiative processes of the donor
58.  $\Gamma^{r, A}$ : rate constants of de-excitation through radiative processes of the acceptor
59.  $\Gamma^{nr, A}$ : rate constants of de-excitation through non-radiative processes of the acceptor
60.  $\Gamma^{RET}$ : rate constants of de-excitation through RET
61.  $[D]_T$ : Total donor concentration
62.  $[A]_T$ : Total acceptor concentration
63.  $m_D$ : Slope of the donor protein solution plot
64.  $m_A$ : Slope of the acceptor protein solution plot
65.  $X_D$ : Molar concentration of donors
66.  $X_A$ : Molar concentration of acceptors
67.  $\tau_X$ : Lifetime of an excited molecule X (where X= donor or acceptor)
68.  $\tau_{XY}$ : Lifetime of an excited molecule X in the presence of an acceptor (X= donor or acceptor, and Y is the opposite species of X)
69.  $R_0$ : Förster distance or radius
70.  $r$ : Distance between a donor and acceptor
71.  $E$ : The amount of excitations dissipated through RET
72.  $P(D)$ : Probability of a monomer to be a donor
73.  $P(A)$ : Probability of a monomer to be an acceptor
74.  $\rho$ : Donor to acceptor ratio
75.  $A(n, \rho)$ : Amplitude of a Gaussian
76. PBS: Phosphate buffer saline

## ACKNOWLEDGEMENTS

First and foremost, I would like to thank Dr. Valerica Raicu for his time, dedication, and pursuit of the betterment of future scientists. Thank you also for allowing me to use many of the derivations of equations that you have found. A similar thank you goes to Dr. Gabriel Biener for his help with the unmixing equations and their derivations, as well as his computer program (OptiMiS DC) to perform such research, and his earliest attempts to get me working experimentally in the lab. Thank you to Dr. Michael Stoneman for his development of the OptiMiS image acquisition software, various analysis tools, and his help with teaching me how to do genetic transformations and prepare cell samples. Thank you to Ashish Mishra for helping me with understanding FRET theory, and providing the dimer and tetramer models, as well as his help with analysis of the meta-histograms. Thank you to Dr. Deo Singh for his help with my understanding of FRET theory, and analysis tools. Thank you to all of these individuals for their time and lengthy discussions that helped to develop this thesis, as well as providing text and figures which led to the final version of this thesis. Thank you also to the rest of the Raicu group and the families of, for all their contributions, this work could not have been done without them, and their support. Lastly, thank you to the University of Wisconsin-Milwaukee faculty and administrators for helping me pursue a Master's Degree in Physics and making it possible.

# Chapter 1

## INTRODUCTION

### ***1.1. History and Background***

Cellular signaling has long been a topic in a variety of fields of research, as it tells us how the basic mechanisms of action within a cell contribute to the whole of the biological kingdom. It wasn't until the last half of the twentieth century that we developed sensitive enough instruments to investigate cellular structure and functions of the internal mechanisms. Cells of all species, whether they be eukaryotic (cells with membrane-bound nucleus) or prokaryotic (cells with non-membrane bound nucleus), have been observed responding to external stimuli since their discovery, but the methods of interaction were also long unknown. The concept of stimuli response, was discovered by an American scientist by the name of Earl W. Sutherland, whose work in the 1950's discovered the mechanisms of action of hormones. He later went on to win the Nobel Prize in Physiology in 1971 for his work with cyclic adenine monophosphate (cAMP), where he proved its intermediary role in many hormonal functions. From this work, he coined the term "second messenger," which referred to the intermediary role the cAMP played in hormonal functions [1].

It was many years later that this work was that an American biochemist, Martin Rodbell worked with a steroid biochemist Oscar Hechter, who influenced Earl W. Sutherland's work, came up with the term "signal transduction." This term referred to how individual cells receive stimuli, process it, and eventually transmit the information within the cell itself. He coined the phrase in 1969 when he began a ten year period of research on the topic. By 1972, his work with guanosine triphosphate (GTP) revealed that GTP itself promoted a release of bound glucagon in the cell, and bound glucagon binding to the cell membrane promoted more

formation of GTP. It was with this GTP molecule that he found stimulation of the guanine nucleotide protein, which was later discovered to be the G-protein. It was this G-protein (or guanine nucleotide-binding protein) that was described by Earl W. Sutherland's "second messenger" system. The G-protein was found to have profound metabolic effects within the cell. For this, he shared the Nobel Prize in Physiology or Medicine in 1994 [2].

The research that followed regarding G-proteins was not fully understood until recent years. It was known by 1988 that G-proteins had receptors along the cellular membrane which interacted with external stimuli. However, it wasn't until 2012, that the entire classification and understanding of G-protein coupled receptors (GPCR's) function was understood. A Nobel Prize was given in chemistry that year to Brian Kobilka and Robert Lefkowitz precisely for this work [3, 4, 5, 6]. Seven other Nobel Prizes have been awarded for various other aspects of G-protein mediated signaling (included are in 1947: Glycogenolysis, 1970: release and reuptake of neurotransmitters, 1971: role of adenylate cyclase and second messenger cyclic AMP, 1988: important principles for drug treatment targeting GPCRs, 1992: reversible phosphorylation activates proteins and regulates cellular processes, 2000: dopamine acts via GPCRs, 2004: work on G-protein-olfactory receptors).

It becomes obvious that G-proteins and their "controllers," the GPCR, are very important to metabolism and cellular function. For this reason, it was an immediate response by the medical and pharmaceutical industry to use these proteins as targets for many drugs. As we jump to current times, the GPCR has been found to be the largest family of transmembrane receptors. They are known as seven-transmembrane receptors due to the passing through of the membrane seven times. Their stimuli can be various, ranging from neurotransmitters, hormones, odors, pheromones, or even light. The stimuli for these receptors is called a ligand, and the interaction of the ligand and the receptor is crucial to cellular function. For this reason,

it is an important source of disease in many organisms when they malfunction, and this is why approximately 40% of all drugs are aimed towards GPCR's [7, 8].

To the scientific community, it has become an ever-important study to discover the structure of GPCRs so that the difference between wild-type, or normal functioning GPCR's, and malfunctioning GPCR's can be distinguished. Also, the binding of the stimuli, or ligand, is vastly important to understanding the release of the G-protein, and whether some obvious structural changes takes place upon this binding of the ligand. The stage was set for scientists to develop ways to analyze the structure of the proteins, whether it be their smallest order of protein folding, known as the primary structure, or their highest, functional order of folding, the quaternary structure. For this reason, physicists have recently crossed over into the realm of biology to become bio-physicists. These biophysicists develop not only the method of detection and measurement, but also the theory behind the biological function and structure. Some modern methods include Fluorescence Recovery After Photo Bleaching (FRAP), X-ray crystallography, and Correlative Light and Electron Microscopy (CLEM) [9, 10, 11, 12].

### ***1.2. Literature Review on a Model GPCR: The Yeast Pheromone Receptor***

There has been much controversy over the relationship between oligomerization and signal transduction, and the functional significance of oligomerization of GPCRs is still unknown. What is known is that certain GPCRs, such as the *d*-opioid receptor, dissociates oligomers upon ligand binding and tends to precede ligand-mediated endocytosis [13]. This indicates that the dissociation of the oligomer plays an important role in endocytosis which leads to signal transduction, or in other words, the second messenger system.

The Sterile-2  $\alpha$ -factor pheromone receptor, or Ste2, is a fungal pheromone mating factor receptor that forms a subcategory of GPCRs. They are integral membrane proteins that

are involved in the response to mating factors found on the cellular membrane [14, 15, and 16]. They contain seven hydrophobic transmembrane domains, which are very similar to other GPCRs, like rhodopsin. Ste2 currently is known to form homo-oligomers and is subject to ligand-mediated endocytosis. Yet it is unknown if it will form hetero-oligomers, and it has been a controversial topic to discuss the size and structure of GPCRs, let alone Ste2. Experiments using detergent to solubilize the  $\alpha$ -factor receptors yielded interesting results about the sedimentation rate. It was found that  $\alpha$ -factor receptors (Ste2, 48 kDa in length) sediment faster than the IgG marker protein (which is 160 kDa in length) [13]. However, the effect of the detergent on the receptor sedimentation rate is unknown pertaining to the hydration, shape, and binding of other proteins.

To understand ligand, or agonist effects, a brief explanation of Ste2 receptor activation and signaling is required. Ste2 is present in two forms within the yeast cell, both a-type and  $\alpha$ -type cells, which use secretion of pheromones to attract the opposite type for mating. By using selective receptors for the pheromone, secreted by the opposite type, the cells can maneuver towards each other and mate. The figure below depicts the sequence in which these events occur.

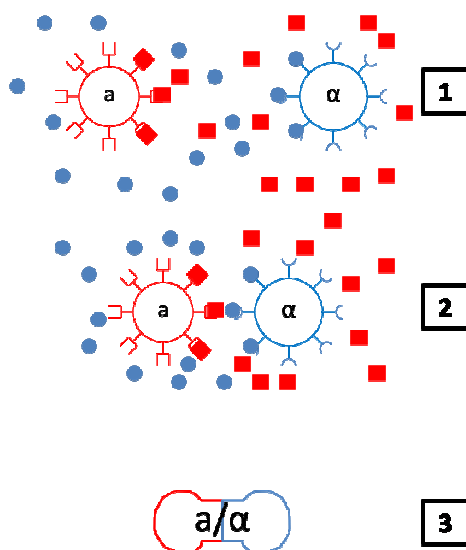


**Figure 1.1.** Schematic representation of how two haploid yeast cells signal to one another via pheromones.

Researchers, Mark C. Overton and Kendall J. Blumer, presented evidence that there may be two ways that the Ste2 might be activated to release the hetero-trimer G-protein [17]. They state that the Ste2 receptor does not hetero-oligomerize with other membrane receptors, but that it is unclear that the size of the homo-oligomer has an effect on the functionality of the receptors. Of the two ways that Ste2 may oligomerize, the first is to consider a dimer of the Ste2 receptor bound to a single G-protein, and the two receptors cooperate to ensure binding of the  $\alpha$ -factor ligand, and hence the release of the G-protein. The second way that Ste2 may oligomerize is to consider the Ste2 forming an oligomer (dimer, tetramer or higher) of Ste2 receptors, and they help stabilize the agonist-bound receptors in its activated conformational state so that one or many of the receptors subunits in a complex can help trigger G-protein release [17]. They are uncertain whether or not the oligomerization can occur in vivo, and that methods that allow for in vivo research are required to explore this. The current research aims to analyze the effect of ligand on oligomerization and conformation of GPCRs, including Ste2, to see if structural changes lead to a release of the G-protein, and hence triggering the signaling pathway.

Consider the two receptor types of each mating species of cell, a-factor mating pheromone receptor, and  $\alpha$ -factor mating receptor. a cells are shown in red, with square receptors, and  $\alpha$  cells are shown with circular receptors. The pheromones for each type are of the same shape as their receptor, square for a, and circles for  $\alpha$ . These pheromones are the ligands for this mating receptor, which in the case of the  $\alpha$  cell, is the  $\alpha$ -factor mating pheromone receptor, or Ste2. In step 1, the cells are near one another and are releasing their mating pheromone. The ligand binds, and the cells move towards the stimuli, or pheromone, as

seen in step 2. Step 3 is when the cells mate and form an  $a/\alpha$  cell. The cells in this experiment are of type  $\alpha$  and will not change to type  $a$  cells, ensuring consistent experimental cells.

### **1.3. Förster Resonance Energy Transfer**

As stated in the previous section of this chapter, intrinsic membrane proteins recognize and respond to a remarkable variety of stimuli that range from light, pressure and other physical agents to molecular ligands such as odorants, hormones, and neurotransmitters. G protein-coupled receptors (GPCRs) form the largest family of such proteins, which interact not only with their eponymous G proteins, but also with GPCRs of their own kind to form homo-oligomers or of a different kind to form hetero-oligomers [18, 19]. While there is a general agreement that many GPCRs form homo-oligomers [18, 20-23], the prevalence, nature, distribution within the cell, the functional relevance of those structures as well the effect of ligand binding on them are subject of considerable debate [24-28].

A variety of methods now exist that approach the problem of protein structure determination in living cells. These include Fluorescence Correlation Spectroscopy (FCS) [29, 30], Fluorescence Recovery After Photobleaching (FRAP) [29], and Spatial Intensity Distribution Analysis (SpiDA) [31, 32]. The in vivo application of Förster Resonance Energy Transfer (FRET) to spectrally resolved two-photon fluorescence microscopy is another method that is used for determination of oligomeric association stoichiometry and quaternary structure. Not only has the laboratory equipment become far more evolved in recent year for all the above mentioned methods, but the analysis has been developed in such a way that creates a cross-examination and verification of the theory with the experimental data. The application of FRET theory in this study is based off the analysis of what is known as the apparent FRET efficiency distribution histogram (or  $E_{app}$  histogram), which is found by plotting the number of image pixels falling in a



certain interval of  $E_{app}$  values against the center of that interval [22, 31, 33]. These histograms are gathered by using a spectrally resolved two photon-microscope system that employs an EMCCD camera that is spectrally resolved at each pixel. The imaged cells are spectrally unmixed using the energy donor (D) and energy acceptor (A) elementary spectra. This yields donor fluorescence intensity in the presence of an acceptor ( $k^{DA}$ ) as well as the acceptor fluorescence intensity in the presence of a donor ( $k^{AD}$ ) at every pixel of the imaged focal plane of the cell [22, 34]. The spatial distribution map of FRET efficiencies was computed based on the  $k^{DA}$  and  $k^{AD}$  values using the equation for *apparent FRET efficiency*, which is derived in Chapter 2 (eq.2.11). This equation relies on six values that are found experimentally, these include the two stated  $k^{DA}$  and  $k^{AD}$  values, the  $w^D$  and  $w^A$ , which are the integrals of the normalized donor and acceptor spectra, and  $Q^D$  (=0.55) is the quantum yield of the donor [22], and  $Q^A$  (=0.61) is the quantum yield of the acceptor [22]. The  $E_{app}$  distributions (or the number of pixels showing a certain FRET efficiency value), or *histogram* as mentioned above, were computed by binning the apparent FRET efficiency values of all the pixels (at a bin size of 0.01). After plotting these histograms they are fit using a theoretical model and their peaks are collected [35]. This is the essence of the method applied in this thesis, however the most recent experiments have aimed to look at effect of averaging of the FRET efficiencies and plotting their values versus the molar concentration of the acceptors. And although this method is constantly developing, many of the finer nuances of the application of FRET theory, such as FRET pair coupling (or the selection process of choosing correct fluorescent tags that attach to the protein to create FRET)[22, 35], spectral overlap in excitation and emission (or how the fluorescent tags excitation spectra only marginally overlap so that only the donor is excited, and how to unmix the emission spectra from both fluorophores) [36], and signal processing(how to remove background noise, apply thresholds to reduce noise, and signal to noise ratio) [22, 35, 33, 37, 38], have all been clearly

established prior to this project. This dissertation aims to focus on the most recent data analysis methods, and thusly the determination of the quaternary structure of the Sterile-2  $\alpha$ -factor receptor protein (Ste2, Ste2p) in the presence and absence of the natural ligand. Ste2 is a GPCR found in the plasma membrane of yeast cells that is a pheromone receptor involved in cellular reproduction through mating, and is important to many fields of research [22, 39].

In a prior investigation [22] into the Ste2 receptor oligomerization, the quaternary structure was determined to be the parallelogram-shaped tetramer. In spite of these results, it was not concluded whether or not this structure was stable or transient associations of dimers. This thesis will focus on the analysis of FRET efficiency histograms in aggregate at first, using a meta-histogram (or a histogram of peak positions of  $E_{app}$  histograms) [33, 40], and then analyzed individually as a function of expression level. The meta-histogram obtained by collecting individual cell histogram peaks in this case allows for the extraction of the peaks that correspond to a dimer, even if the background of signals is from higher order oligomers. The investigation into individual histograms to fit them with a tetrameric model results in a best fit using the parallelogram shaped tetramer model. The thesis presented aims to show that both stable dimers and dynamically associated tetramers of Ste2 may coexist within living yeast cells, regardless of the presence and absence of the ligand.

## Chapter 2

### MATERIALS AND METHODS

#### 2.1 Sample Preparation

##### 2.1.1. Genetic Constructs

Two variations of the green fluorescent protein (GFP) were used in tagging the receptor of interest. The natural or wild type GFP excites at 395 nm, whereas, the variant used to tag the energy donor (due to excitation) was GFP<sub>2</sub>. The excitement peak of GFP<sub>2</sub> differs from that of the wild-type by having shifted to 398 nm. The cause for this is the addition of the amino-acid substitute F64L [41]. GFP<sub>2</sub> was created by site-directed mutagenesis which caused nucleotide change to result in the substitution of F64L in the protein. The wild-type GFP is from *Aequorea Victoria*, which was provided by J. Greenblatt of the University of Toronto. Ste2 receptors were tagged with the energy acceptor, which is the yellow fluorescent protein (YFP), adjusted with the amino-acid S65G S72A T203Y, which has a maximum excitation peak at 520 nm [22, 38, 42].

The Sterile 2  $\alpha$ -factor receptor protein (Ste2p or Ste2) used in this experiment were individually fused with both GFP<sub>2</sub> and YFP at the same 304 position in the amino acid sequence. Eight of the amino acids of the cytoplasmic tail of the Ste2 were removed, resulting in increased FRET efficiency. The plasmids expressing Ste2 were inserted into a strain of *Saccharomyces Cerevisiae* which expressed a non-functioning copy of Ste2 within the chromosome (KBY58; MATa leu2–3,112, ura3–52 his3– $\Delta$ 1 trp1 sst1– $\Delta$ 5 ste2 $\Delta$ ). The particular yeast used was the type a [43] mating haploids, which contains a mutation (ho) to prevent the cells from switching from type a to type  $\alpha$ . This mutation allows for the use of ligand ( $\alpha$ -factor) without effecting homo-oligomerization [39].

### 2.1.2. Cell Growth

Baker's yeast cells (*Saccharomyces cerevisiae*) expressing one or both of the plasmids that induce growth of GFP<sub>2</sub> and YFP were grown on a petri dish consisting of synthetic-complete solid medium (agar) which lacked either uracil, or both uracil and tryptophan, allowing for the selection of the plasmid of interest. The plasmids used are VR1988, which contains Ste2 tagged with GFP<sub>2</sub> and lacks the uracil amino acid, the plasmid VR2033 contains Ste2 tagged with YFP and lacks the tryptophan amino acid, the plasmid VR2051 contains Ste2 but is not tagged with any fluorescent protein and lacks the uracil amino acid, and lastly, the VR2052 contains Ste2 but is not tagged with any fluorescent protein and lacks the tryptophan amino acid. The variations transformed were as follows: VR1988 and VR2033 to make cells that express Ste2 tagged with both fluorophores, VR1988 and VR2052 to make cells that express Ste2 tagged with only GFP<sub>2</sub>, VR2033 and VR2051 to make cells that express Ste2 tagged with only YFP, and a control culture that contained no plasmids. The plates were incubated for five days at 30° C. After incubating for five days, two types of cell suspension were prepared (ligated and non-ligated) from the plates using the following protocol. Multiple yeast cell colonies (5-7) were scraped from the solid medium and resuspended in 800  $\mu$ L of 100 mM KCl (to maintain neutral pH which ensures constant quantum yield of the fluorescent molecules). To one of the volumes (denoted as ligated), 0.8  $\mu$ L of 10 mM  $\alpha$ -factor in 100 mM sodium acetate solution was added (Zymo Research Corporation, Orange, CA, U.S.A.); the final concentration of the  $\alpha$ -factor ligand in the ligated cellular suspension was 10  $\mu$ M. To replicate this treatment, save for the addition of the  $\alpha$ -factor, 10  $\mu$ L of 100 mM sodium acetate solution was added to the other volume of cells (denoted as non-ligated). After an incubation time of 10 minutes, 200  $\mu$ L of cells were drawn from each of the two suspensions and pipetted onto the surface of separate uncoated glass bottom dishes (Matsunami Glass Ind., Ltd, Osaka, Japan). Both dishes were taken to the imaging

system (see Two-photon fluorescence micro-spectroscopy section below), where individual cells were randomly located, scanned with the excitation beam, and their fluorescence emission collected. Imaging was alternated between the ligated and non-ligated dishes every 50 minutes, until ~500 cells were imaged from each dish. Alternating between the two dishes assured that there would be no observable effects due to a difference in time after the cell suspensions were prepared.

For the most recent experiments involving two wavelength excitation and presence and absence of ligand, cells were treated identically above, but were placed on the same dishes that were coated with Concanavalin A (described in detail in the *Adherence and Immobilization of Yeast Cells for Imaging* section of the *Materials and Methods*). The cells were placed on these coated dishes and 10 minutes were allowed to pass before imaging to ensure adherence.

Introduction of ligand in this last experiment required the same concentration of  $\alpha$  - factor in the same solution. However, cells were presented with only potassium chloride and sodium acetate before the ligand to generate the cell suspension. The amount of cell suspension added to each dish for imaging was 200  $\mu$ L and after being imaged at two wavelengths the solution was then removed from the dish with the adherent cells. Then the  $\alpha$ -factor solution was administered in the same volume of 200  $\mu$ L and imaged again at both wavelengths.

### *2.1.3. Adherence and Immobilization of Yeast Cells for Imaging*

More recent experiments required imaging of yeast cells before and after the introduction of ligand. *Sacchomyces Cerevisiae* is difficult to image due to being a non-adherent form of yeast that can easily be moved by variations in thermal convection flow within cultures or from introduction of other solutions into the cell suspension. However, due to the expense limitation

of complicated microfluidic devices that were explored (EMD Millipore CellASIC® ONIX Microfluidic Platform, Ballerica, MA, U.S.A.), alternative methods of cell capturing were explored. One method which has been used by many research groups [44, 45] is the coating of imaging slides or dishes with a soybean lectin product called Concanavalin A, or Con A. The protocol for creating Con A dishes used in the latest experiments is as follows:

1. 2 mg of Concanavalin A (C7898-10MG, Sigma-Aldrich, St. Louis, MO, U.S.A.) was measured and placed into a glass jar containing 4 mL of autoclaved, deionized water and was mixed thoroughly.
2. Sterile Non-Coated Glass –Bottom Matsunami Dishes (Matsunami Glass Ind., Ltd, Osaka, Japan) were laid out on a sterile surface, and the cover was removed.
3. 100  $\mu$ L of the aqueous Con A solution was placed onto the dish and covered immediately. 30 minutes was allowed to pass to let deposition occur.
4. The remaining solution was removed from the dishes and discarded. Then the dishes were allowed to dry completely, and stored in a sterile plastic wrap covered with aluminium foil until ready for imaging.
5. Dishes were labelled according to their order in which they would be imaged.
6. Cell solutions were created as described in the *Sample Preparation* section of the *Materials and Methods*, and were placed on the dish in volumes of 200 $\mu$ L.
7. 10 minutes were allowed to pass to ensure cell deposition and adherence.
8. Cells were imaged at both wavelengths, and then the solution was removed, leaving only the cells.
9. Ligand solution was then administered without moving the dish, and the same cells were imaged at both wavelengths.

10. Dishes and cells were then discarded, and the process would repeat until the experiment was finished.

## ***2.2. Two-Photon Fluorescence Micro-Spectroscopy***

A single pulsed laser was used as the excitation light source for this experiment (SpectraPhysics MAITAI One Box Tunable laser, Santa Clara, CA). The laser is an ultra-short-pulsed (100 femtosecond), mode-locked, Ti: Sapphire laser that runs at 80 MHz and is tunable between ~690 to 1040 nm. The full-width half maximum of the laser is ~7 nm. The laser light was focused with an infinity-corrected Plan Apochromat lens (x100 magnification, NA=1.4, using immersion oil, Nikon Instruments, Melville, NY, U.S.A.). The microscope objective was mounted to a Nikon Eclipse Ti-Series using the Optivar 1.5x magnification (Nikon Instruments, Melville, NY). The light was scanned using galvanometric scanners (Nutfield Technology, Hudson, NH) and non-descanned detection was used. OptiMis TruLine employs a line-scan protocol that leads to signals two orders of magnitude higher than that of a point-scan-based system using the same line dwell time [46]. The excitation power was measured using a photodiode detector placed at the turret objective aperture and was measured to be 800mW at 800nm for the first portion of this experiment, then measured to be 300mW at both 800nm and 960nm (for the dual excitation experiment). The light from the fluorescing tags was projected through a transmission grating onto a -70 degree Celsius electron-multiplying charged-coupled device (EMCCD) camera that achieves single-photon sensitivity (iXon3 897; Andor Technology, South Windsor, CT). The different wavelengths of light composing the emitted fluorescence are separated as a function of pixel position on the CCD array. Therefore, the signal captured by the OptiMiS detection system contains three-dimensional information; two of the dimensions are spatial dimensions (300 x 200 pixels for the first experiment, 440 x 200 pixels for the second),

and the third dimension is wavelength, i.e. each pixel in the 2D image is sampled at 200 different wavelength channels. The spectral bandwidth ranges from 415 nm to 615 nm with a spectral resolution of 1 nm. The use of a high-speed EMCCD camera allows for the observance of time scales that are far shorter than the molecular diffusion time scales [22]. This feature is needed when imaging live cells at the molecular level using two-photon microscopy. The system is also calibrated using a known fluorophore called fluorescein, which emits a consistent emission spectra which is compared to the known spectra based on the literature. In this experiment, the system was set to take an image of 300(x-pixels) by 200(y-pixels) at a spectral acquisition dwell time of 100 microseconds and at a spectral resolution of 1 nanometer. Since the system uses a line scan method, each line dwell time was set 50  $\mu$ s for the first experiment and 35  $\mu$ s for the second, and the total acquisition time for a full set of spectrally resolved images (for example 440x200 pixels, 200 wavelengths per pixel) was  $\sim$ 7 seconds.

### ***2.3. Choosing the FRET Pairs***

Since the microscope system is that of a two-photon type, it requires that the wavelength be selected at exactly half of that which you are trying to excite at. In this case, GFP<sub>2</sub> was used as the donor of energy, and has an excitation maximum at  $\sim$ 400 nm [42, 47], hence two photon excitation at  $\sim$ 800 nm. GFP<sub>2</sub> also has large Stokes shift, and hence avoids direct excitation of the acceptor, a crucial factor when determining FRET pairs. The acceptor in this experiment was chosen to be YFP since its excitation spectrum overlaps directly with the emission spectrum of the donor. YFP also has a two-photon excitation maximum at  $\sim$ 1020 nm [22, 38, 42], which means it cannot be directly excited by the laser emission at  $\sim$ 800 nm. Furthermore, the laser was checked for full-width half maximum (FWHM) and achieved  $\sim$ 30 nm, helping to verify the absence of overlap in excitation.



## 2.4. Emission Spectra

Yeast cells expressing the Ste2 protein tagged with the GFP<sub>2</sub> and YFP are placed on 35mm Matsunami glass bottom dishes (non-coated) and placed on the x-y-z stage of the microscope and placed on top of the objective using immersion oil of the same NA as the glass on the bottom of the glass bottom dish. The spectral images of the GFP<sub>2</sub> were obtained by using the 800nm pulsed laser that had a mean power of ~1.1W at the exit of the laser. Emission spectra were obtained for several cells expressing only the GFP<sub>2</sub> tag. The spectra were averaged and normalized with respect to their maximum emission intensities to obtain the normalized spectrum for the GFP<sub>2</sub> donor (D). Similarly, the emission spectra for the acceptor-only tagged yeast cells were obtained and averaged and normalized. This time, the acceptor (A) is YFP, which has a red-shifted excitation spectrum, requires 955nm excitation and nearly double the power because YFP does not absorb as efficiently at 800nm.

## 2.5. Unmixing of Measured Fluorescence Spectra

To properly analyze the emission fluorescence gathered by the system, “unmixing” of the elementary spectra coming from both fluorescent tags is required. A single pixel within a 2D fluorescent image contains a power spectrum arising from the emission of fluorescent molecules that are contained within the sample voxel corresponding to that particular pixel. Therefore, the measured power spectrum is a linear combination of the power spectra of the individual fluorescent tags, which can be denoted by  $S_1, S_2, \dots, S_l$ , multiplied by a coefficient proportional to the concentration of the corresponding fluorescent tag, i.e.  $k_1, k_2, \dots, k_l$

Thus the measured power spectrum can be written as:

$$P = \bar{S} \cdot k + n, \quad (2.1)$$

where  $\mathbf{P}$  is the measured intensity spectrum vector for  $m$  wavelength channels,  $\mathbf{n}$  is the experimental noise term coming from the camera noise or random external noise, which is treated as Gaussian noise where the mean value is zero and has a standard deviation (essentially a first order approximation), and  $\bar{\mathbf{S}} = [\mathbf{S}_1 \mathbf{S}_2 \dots \mathbf{S}_m]$  is the  $m \times l$  matrix composed of the  $l$  individual spectra of the fluorescent tags placed side by side in a matrix with each tag having  $m$  measured wavelength channels, and  $\mathbf{k} = [k_1 k_2, \dots, k_l]$  is a vector of the coefficients. Our goal is to extract the  $\mathbf{k}$  vector which will give us an indication of the amount of fluorescent molecules residing within a particular excitation voxel for each fluorescent tag. This was accomplished by using a least squares minimization procedure, i.e.:

$$\min_{\mathbf{k}} \|\mathbf{P} - \bar{\mathbf{S}} \cdot \mathbf{k}\|_2^2 \quad (2.2)$$

Eq. (2.2) represents the minimal value of the second norm square of the expression within  $\|\cdot\|$ . Taking the derivative of the expression to be minimized by  $\mathbf{k}$ , equating to zero, and rearranging the equation yields:

$$\mathbf{k} = (\bar{\mathbf{S}}^T \cdot \bar{\mathbf{S}})^{-1} \cdot \bar{\mathbf{S}}^T \cdot \mathbf{P} \quad (2.3)$$

The superscript  $^T$  indicates the transpose of the matrix. The quantities on the right side of eq. (2.3) are measured, while  $\bar{\mathbf{S}}$  was measured by imaging cells transformed with a single type of plasmid, i.e. either Ste2-GFP<sub>2</sub> only or Ste2-YFPonly. The spectrum for each measured tag was normalized to its maximum.  $\mathbf{P}$  as mentioned above is the measured pixel power spectrum along  $m$  channels.

In order to reduce the pixel non-uniformity of the measuring system we consider a tag which we call background tag. This artificial tag is plugged into Eq. (2.3) as a third tag which has a unity power spectrum across the  $m$  channels.

Spectral images obtained from cells co-expressing Ste2p-GFP<sub>2</sub> and Ste2p-YFPproteins were unmixed (described above) using  $S_D$  (elementary donor power spectrum) and  $S_A$  (elementary acceptor power spectrum) to obtain separate donor (denoted by  $k_1 = k^{DA}$ ) and acceptor ( $k_2 = k^{AD}$ ) images. The apparent FRET efficiency ( $E_{app}$ ) distribution in a given optical section of an imaged cell, as calculated using eq. (2.11), was determined for each image pixel using  $k^{DA}$ ,  $k^{AD}$ ,  $w^A$  and  $w^D$  (which are the integrals of the measured elementary spectra of A and D, respectively), and  $Q^D$  and  $Q^A$  which are the quantum yields of D and A, respectively, and the quantum yield values ( $Q^D = 0.55$  and  $Q^A = 0.61$ ) were obtained from the literature [22, 32]. It should be noted, that to arrive at eq. (2.11) in chapter 2.6.3, it is assumed that direct excitation of the acceptor fluorophore is negligible. The computations, for both spectral unmixing and  $E_{app}$  determination, were performed using a program written in house using Matlab (MathWorks Inc., USA). Pseudo-FRET efficiencies for pixels showing only background noise were avoided by setting  $E_{app}=0$  for the pixels characterized by signal to noise ratios less than one standard deviation of the noise for both donor and acceptor signals.

## **2.6. Signal Unmixing Details and Method**

### **2.6.1. Threshold Based on Signal to Noise Ratio**

The threshold processes is performed as follows:

- a. The unmixing is calculated using the method described earlier for each pixel.
- b. We multiply the computed  $k$  vector with the measured  $\bar{S}$  matrix, which would give us the fitted curve.
- c. We then subtract the fitted curve from the measured spectrum and end up with the noise term.

- d. We then calculate the noise distribution's standard deviation,  $\sigma$ , and the mean should turn out to be zero.
- e. After calculating  $\sigma$  we compare it to the maximum signal portion coming from each individual tag that participates in the FRET processes. If the maximum of the signal is below  $Th \cdot \sigma$  for either of the tags, then this pixel is disregarded, otherwise the pixel is considered.  $Th$  is the chosen threshold which is based on  $E_{app}$  image sharpness.

The threshold for the above described process was 1.

### *2.6.2. Fluorescence Background Subtraction*

In the biological system discussed in this paper, we are using two fluorescent molecules, GFP<sub>2</sub> used as a donor and YFP as an acceptor. These molecules are used for tagging the protein of interest which is Ste2. Moreover, additional emission can come from auto-fluorescence or introduced by the cells or background emission that can result from either white light illumination penetrating the system or pixel non-uniformity. The auto-fluorescence in the presented system is negligible; however, we decided to still consider the background. Using the method described above we can unmix and subtract the background intensity distribution. The subtraction can be performed by assuming that the background is one of the fluorescent tags. The normalized spectrum of that virtual tag, within the first order approximation, is unity for all the measured wavelengths.

### *2.6.3. Theory of the Method*

Many of the figures in this thesis rely solely on emissions coming from only that of the donor molecules. This was used to determine concentration and to attempt to derive the oligomeric structure based on other analyses using the data already collected through the spectrometer or

EMCCD. Through careful measurements of various emissions at certain excitation wavelengths, one can derive the loss of donor emission due to FRET, or  $F^D(\text{FRET})$ . The equation is

$$F^D(\text{FRET}) = F^A(\text{FRET}) Q^D / Q^A \quad (2.4)$$

where  $Q^D$  and  $Q^A$  are the quantum yields as discussed in the Chapter 2.5, and  $F^A(\text{FRET})$  is loss of acceptor emission through FRET. Not only were apparent FRET efficiencies used to analyze the oligomeric structure, but also the donor only emission as predicted by FRET theory. Starting with the expression for the total number of photons emitted from both fluorescent species in the presence of FRET

$$F^{\text{DA}}(\lambda_{\text{ex}}) + F^{\text{AD}}(\lambda_{\text{ex}}) = F^{\text{D}}(\lambda_{\text{ex}}) - F^{\text{D}}(\text{FRET}) + F^{\text{A}}(\lambda_{\text{ex}}) + F^{\text{A}}(\text{FRET}) \quad (2.5)$$

where,

$$F^{\text{DA}}(\lambda_{\text{ex}}) = k^{\text{DA}}(\lambda_{\text{ex}}) \int_{\lambda_{\text{em}}} i^{\text{D}}(\lambda_{\text{em}}) d\lambda_{\text{em}} = k^{\text{DA}}(\lambda_{\text{ex}}) w^{\text{D}} \quad (2.6)$$

and,

$$F^{\text{AD}}(\lambda_{\text{ex}}) = k^{\text{AD}}(\lambda_{\text{ex}}) \int_{\lambda_{\text{em}}} i^{\text{A}}(\lambda_{\text{em}}) d\lambda_{\text{em}} = k^{\text{AD}}(\lambda_{\text{ex}}) w^{\text{A}} \quad (2.7)$$

which were previously derived by Raicu et. al [34].  $F^{\text{DA}}(\lambda_{\text{ex}})$  is the number of photons emitted by the donor (D) in the presence of the acceptor (A) as measured at the excitation wavelength  $\lambda_{\text{ex}}$ .  $F^{\text{AD}}(\lambda_{\text{ex}})$  is the number of photons emitted by the acceptor

in the presence of the donor at the excitation wavelength  $\lambda_{\text{ex}}$ .  $k^{\text{DA}}(\lambda_{\text{ex}})$  is a component of calculation of  $F^{\text{DA}}$ , and likewise  $k^{\text{AD}}(\lambda_{\text{ex}})$  is a component of calculation of  $F^{\text{AD}}$ .

This leaves  $i^{\text{A}}(\lambda_{\text{em}})$  and  $i^{\text{D}}(\lambda_{\text{em}})$ , which are the emission spectrum normalized to one of acceptors and donors. Also,  $w^{\text{D}}$  and  $w^{\text{A}}$  are the integrals of elementary spectra of both donor and acceptors, respectively.

Next, Equation (2.5) can be separated into equations that describe only  $F^{\text{DA}}$  or  $F^{\text{AD}}$  by extracting only the terms that pertain to the donor, or only the acceptor. Here,  $F^{\text{D}}(\lambda_{\text{ex}})$  is the donor emission in the absence of FRET.

$$F^{\text{DA}}(\lambda_{\text{ex}}) = F^{\text{D}}(\lambda_{\text{ex}}) - F^{\text{D}}(\text{FRET}) \quad (2.8)$$

and

$$F^{\text{AD}}(\lambda_{\text{ex}}) = F^{\text{A}}(\lambda_{\text{ex}}) + F^{\text{A}}(\text{FRET}) \quad (2.9)$$

Thus allowing to solve for  $F^{\text{D}}(\text{FRET})$  which is the fluorescence emission of the donor lost due to the presence of FRET which is equation 2.4 where  $Q^{\text{D}}$  and  $Q^{\text{A}}$  are the quantum yields as discussed in Chapter 2.5. These values were used to find  $F^{\text{D}}(\text{FRET})$  or  $F^{\text{D}}$  which was used in various portions of this paper to determine concentration of molecules based on the donor only emission in the presence of FRET. The apparent FRET efficiency is then given by:

$$E_{\text{app}} = \frac{F^{\text{D}}(\text{FRET})}{F^{\text{D}}(\lambda_{\text{ex}})} \quad (2.10)$$

or likewise,

$$E_{app} = \left[ 1 + \frac{Q^A w^D k^{DA}}{Q^D w^A k^{AD}} \right] \quad (2.11)$$

Note that equation 2.11 is a special case of using only one excitation wavelength. Yeast cells were transformed to express Ste2 receptors with GFP<sub>2</sub>-tagged and YFP-tagged proteins to determine whether they self-associate to form oligomers. Spectral images obtained from cells expressing Ste2 with both GFP<sub>2</sub>-tagged and YFP-tagged proteins were unmixed using the various software platforms to obtain separate donor (denoted by  $k^{DA}$ ) and acceptor ( $k^{AD}$ ) images, as described in previous publications[33, 34, 35, 37, 38, 47]. The apparent FRET efficiency ( $E_{app}$ ) distribution of an imaged cell by selection of an area cross-section of the cell was determined for each image pixel using  $k^{DA}$  and  $k^{AD}$  and the equation 2.11, where  $w^A$  and  $w^D$  are the integrals of the measured elementary spectra of the acceptors fluorophores and donor fluorophores, respectively.  $Q^D$  and  $Q^A$  are the quantum yields of D and A, respectively [37, 41], and their values ( $Q^D = 0.55$  and  $Q^A = 0.61$ ) were obtained from previous publications as well [22]. All the computations were performed using the Matlab program (The MathWorks, Inc., USA) and an in house software called OptiMiS Data Cruncher or OptiMiS DC (Courtesy of Dr. Gabriel Biener of the Raicu Group). Pseudo-FRET efficiencies for pixels showing only background noise were avoided by use of a threshold within the program that is based off of the signal to noise ratio (described below).

## **2.7. Determination of Donor and Acceptor Concentrations**

The second explorative experiments were done in an effort to approximate donor and acceptor concentration within living cells, as well as use that concentration information to see there was an effect on average  $E_{app}$  for each cell in the absence and presence of the ligand. To determine

the concentrations of donors and acceptors, information that was not available in previous experiments was required. The primary driver of this experiment was specifically the acceptor concentration, or more specifically acceptor molar concentration. However, to find this information, exciting the cells at both the donor maxima and the acceptor maxima was required. Hence, a dual excitation scheme was adopted to gather this information. Once the cells were immobilized, as described in the *Adherence and Immobilization of Yeast Cells for Imaging* portion of the *Materials and Methods* section, the same cells could be dually excited in the absence and presence of the ligand. First, cells were added to Con A coated dishes and imaged at both 800 nm and 960 nm excitations with laser power equal to 300 mW for both scans. Second, the solution was removed, and ligand solution was added, and again the same cells were imaged at 800 nm and 960 nm at the same power of 300 mW for both scans. Over 19 fields of view were scanned for each wavelength and in the absence and presence of the ligand, collecting a number of cells in each field of view. Once the raw data was collected, the images were spectrally unmixed using OptiMiS DC software described in the *Unmixing* section of the *Materials and Methods*. The 800 nm data before ligand introduction was unmixed, only selecting the membrane with a region of interest. After collecting numerous membranes of various cells within each field of view, the regions of interest were saved and used later on the other data to maintain the same numbers of pixels used for averaging. Next, the other data was unmixed that contained 960 nm in the absence of ligand, and 800 nm and 960 nm in the presence of ligand. The software gives an output of  $k^{DA}$ ,  $k^{AD}$ ,  $E_{app}$ , and  $F^D$  only images, as well as histograms of each region of interest taken. For the analysis of averaging  $E_{app}$  and calculating donor and acceptor molar concentrations, we need only the information from the  $k^{DA}$  and  $k^{AD}$  images.



Using the unixed data sets, we would now take the  $K^{AD}$  measurements (which are now in .tif format) and insert them into ImageJ, and using the region of interest manager, import the regions of interest selected when unmixing the first set of 800 nm data. Now, ImageJ would be used to measure the intensity via histogram, this data would be then moved to Microsoft Excel for later analysis. Before any calculations were made, discarding the pixels with zero intensity ensured an average that was only of actual photon counts, not zero intensity counts. Also, there was no thresholding done to the  $K^{DA}$  and  $K^{AD}$  images since each should represent only real photons being counted by the camera for those spectra.

To understand the method of obtaining the molar concentration and average  $E_{app}$ , we must start with the mathematics. The derivations herein are provided by Dr. Michael Stoneman and Dr. Valerica Raicu. Starting from the FRET equation for  $E_{app}$ :

$$E_{app} = \frac{F^D(RET, \lambda_1)}{F^D(\lambda_1)} = \frac{F^D(\lambda_1) - F^{DA}(\lambda_1)}{F^D(\lambda_1)} = 1 - \frac{F^{DA}(\lambda_1)}{F^D(\lambda_1)} \quad (2.12)$$

The  $E_{app}$  equation relies on the donor fluorescence intensity due to resonant energy transfer (RET) at the first wavelength, or  $F^D(RET, \lambda_1)$ , and donor fluorescence only at wavelength one  $F^D(\lambda_1)$ . But  $F^D(RET, \lambda_1)$  can be rewritten as  $F^D(\lambda_1) - F^{DA}(\lambda_1)$ , where  $F^{DA}(\lambda_1)$  is the donor fluorescence intensity in the presence of an acceptor at the first wavelength, accounting for the transfer due to RET, and hence we see a reduced equation. Now, assuming we can obtain rates of excitation of acceptors only at a first and second wavelength, then  $\Gamma_{ex}^{\lambda_1, A}$  is the rate of excitation of the acceptor at the first wavelength, and  $\Gamma_{ex}^{\lambda_2, A}$  is the rate of excitation of the acceptor at the second wavelength. Similarly, we can obtain the rates of excitation of the donors only at the first and second wavelength, then then  $\Gamma_{ex}^{\lambda_1, D}$  is the rate of excitation of the donor at the first wavelength, and  $\Gamma_{ex}^{\lambda_2, D}$  is the rate of excitation of the donor at the second wavelength. Then we can obtain

Gamma ratios of either the donor from donor only expressing cells (GDR) or the acceptor from acceptor only expressing cells (GAR), or  $\frac{\Gamma_{ex}^{\lambda_2,D}}{\Gamma_{ex}^{\lambda_1,D}}$  and  $\frac{\Gamma_{ex}^{\lambda_2,A}}{\Gamma_{ex}^{\lambda_1,A}}$ , respectively. Now, we need some

fundamental groups of equations to derive the concentrations of donors and acceptors:

Fundamental Group 1:

$$F^{DA}(\lambda_1) = F^D(\lambda_1) - F^D(RET, \lambda_1) \quad (2.13)$$

$$F^{AD}(\lambda_1) = F^A(\lambda_1) + F^A(RET, \lambda_1) \quad (2.14)$$

$$F^{DA}(\lambda_2) = F^D(\lambda_2) - F^D(RET, \lambda_2) \quad (2.15)$$

$$F^{AD}(\lambda_2) = F^A(\lambda_2) + F^A(RET, \lambda_2) \quad (2.16)$$

Fundamental Group 2:

$$F^D(RET, \lambda_1) = \Gamma_{ex}^{\lambda_1,D} \cdot Q^D \cdot \mu_{olig} \cdot E_{olig} \quad (2.17)$$

$$F^D(RET, \lambda_2) = \Gamma_{ex}^{\lambda_2,D} \cdot Q^D \cdot \mu_{olig} \cdot E_{olig} \quad (2.18)$$

$$F^D(RET, \lambda_2) = \frac{\Gamma_{ex}^{\lambda_2,D}}{\Gamma_{ex}^{\lambda_1,D}} \cdot F^D(RET, \lambda_1) \quad (2.19)$$

Fundamental Group 3:

$$F^D(\lambda_1) = \Gamma_{ex}^{\lambda_1,D} \cdot Q^D \cdot [D]_T \quad (2.20)$$

$$F^D(\lambda_2) = \Gamma_{ex}^{\lambda_2,D} \cdot Q^D \cdot [D]_T$$

(2.21)

$$F^A(\lambda_1) = \Gamma_{ex}^{\lambda_1, A} \cdot Q^A \cdot [A]_T$$

(2.22)

$$F^A(\lambda_2) = \Gamma_{ex}^{\lambda_2, A} \cdot Q^A \cdot [A]_T$$

(2.23)

Relationship 1:

$$F^D(\lambda_2) = \frac{\Gamma_{ex}^{\lambda_2, D}}{\Gamma_{ex}^{\lambda_1, D}} \cdot F^D(\lambda_1)$$

(2.24)

$$F^A(\lambda_2) = \frac{\Gamma_{ex}^{\lambda_2, A}}{\Gamma_{ex}^{\lambda_1, A}} \cdot F^A(\lambda_1)$$

(2.25)

Relationship 2:

$$F^D(RET, \lambda_1) = \frac{Q^D}{Q^A} \cdot F^A(RET, \lambda_1)$$

(2.26)

$$F^D(RET, \lambda_2) = \frac{Q^D}{Q^A} \cdot F^A(RET, \lambda_2)$$

(2.27)

Now, from these assumptions we can calculate FRET efficiency as per eq. 2.12. To get donor concentration we need  $F^D(\lambda_1)$  and using eq 2.13 we can rewrite it as

$$F^D(\lambda_1) = F^{DA}(\lambda_1) + F^D(RET, \lambda_1)$$

and using eq. 2.26

$$F^D(\lambda_1) = F^{DA}(\lambda_1) + \frac{Q^D}{Q^A} \cdot F^A(RET, \lambda_1)$$

and using eq. 2.14

$$F^D(\lambda_1) = F^{DA}(\lambda_1) + \frac{Q^D}{Q^A} [F^{AD}(\lambda_1) - F^A(\lambda_1)]$$

Rearrange

$$F^D(\lambda_1) = F^{DA}(\lambda_1) + \frac{Q^D}{Q^A} \cdot F^{AD}(\lambda_1) - \frac{Q^D}{Q^A} \cdot F^A(\lambda_1)$$

Now, if  $F^A(\lambda_1)$  can be assumed to be zero, then this can be determined from measurements,

but if not, then using eq. 2.25 the equation becomes

$$F^D(\lambda_1) = F^{DA}(\lambda_1) + \frac{Q^D}{Q^A} \cdot F^{AD}(\lambda_1) - \frac{Q^D}{Q^A} \cdot \frac{\Gamma_{ex}^{\lambda_1,A}}{\Gamma_{ex}^{\lambda_2,A}} \cdot F^A(\lambda_2)$$

and  $F^A(\lambda_2)$  is found from rearranging eq. 2.16

$$F^A(\lambda_2) = F^{AD}(\lambda_2) + F^A(RET, \lambda_2)$$

and using eq. 2.27

$$F^A(\lambda_2) = F^{AD}(\lambda_2) - \frac{Q^D}{Q^A} \cdot F^D(RET, \lambda_2)$$

and using eq. 2.19

$$F^A(\lambda_2) = F^{AD}(\lambda_2) - \frac{Q^D}{Q^A} \cdot \frac{\Gamma_{ex}^{\lambda_2,D}}{\Gamma_{ex}^{\lambda_1,D}} \cdot F^D(RET, \lambda_1)$$

then eq. 2.27 becomes

$$F^A(\lambda_2) = F^{AD}(\lambda_2) - \frac{\Gamma_{ex}^{\lambda_2,D}}{\Gamma_{ex}^{\lambda_1,D}} \cdot F^A(RET, \lambda_1)$$

and plug into eq. 2.14

$$F^A(\lambda_2) = F^{AD}(\lambda_2) + \frac{\Gamma_{ex}^{\lambda_2,D}}{\Gamma_{ex}^{\lambda_1,D}} \cdot [F^{AD}(\lambda_1) - F^A(\lambda_1)]$$

and if  $F^A(\lambda_2)$  is assumed to be zero, then everything in the above equation can be determined

from measurements. If we don't make this assumption, then rearrange

$$F^A(\lambda_2) = F^{AD}(\lambda_2) - \frac{\Gamma_{ex}^{\lambda_2,D}}{\Gamma_{ex}^{\lambda_1,D}} \cdot F^{AD}(\lambda_1) + \frac{\Gamma_{ex}^{\lambda_2,D}}{\Gamma_{ex}^{\lambda_1,D}} \cdot F^A(\lambda_1)$$

and using eq. 2.27 becomes

$$F^A(\lambda_2) = F^{AD}(\lambda_2) - \frac{\Gamma_{ex}^{\lambda_2,D}}{\Gamma_{ex}^{\lambda_1,D}} \cdot F^{AD}(\lambda_1) + \frac{\Gamma_{ex}^{\lambda_2,D}}{\Gamma_{ex}^{\lambda_1,D}} \cdot \frac{\Gamma_{ex}^{\lambda_1,A}}{\Gamma_{ex}^{\lambda_2,A}} \cdot F^A(\lambda_2)$$

rearrange this equation

$$F^A(\lambda_2) \left( 1 - \frac{\Gamma_{ex}^{\lambda_2,D}}{\Gamma_{ex}^{\lambda_1,D}} \cdot \frac{\Gamma_{ex}^{\lambda_1,A}}{\Gamma_{ex}^{\lambda_2,A}} \right) = F^{AD}(\lambda_2) - \frac{\Gamma_{ex}^{\lambda_2,D}}{\Gamma_{ex}^{\lambda_1,D}} \cdot F^{AD}(\lambda_1)$$

so now we have a fully measurable  $F^A(\lambda_2)$  by rearranging into

$$F^A(\lambda_2) = \frac{F^{AD}(\lambda_2) - \frac{\Gamma_{ex}^{\lambda_2,D}}{\Gamma_{ex}^{\lambda_1,D}} \cdot F^{AD}(\lambda_1)}{1 - \frac{\Gamma_{ex}^{\lambda_2,D}}{\Gamma_{ex}^{\lambda_1,D}} \cdot \frac{\Gamma_{ex}^{\lambda_1,A}}{\Gamma_{ex}^{\lambda_2,A}}}$$

which allows for the calculation of acceptor concentration by eq. 2.23

$$[A]_T = \frac{F^A(\lambda_2)}{\Gamma_{ex}^{\lambda_2,A} \cdot Q^A} = \frac{F^{A \text{ only}}(960)}{m_A}$$

(2.28)

and use  $\lambda_2$  measurement on solution of proteins at known concentration to obtain  $\Gamma_{ex}^{\lambda_2,A}$  and

where  $m_A = \text{Slope}(A) = \Gamma^{960,A} \cdot Q^A$  is the slope of the line which is the measurements of

intensities at various concentrations of acceptor protein solutions.

Now we need to derive the donor concentration accounting for  $F^A(\lambda_2)$  not equal to zero. Using eq. 2.25  $F^D(\lambda_1)$  becomes

$$F^D(\lambda_1) = F^{DA}(\lambda_1) + \frac{Q^D}{Q^A} \cdot F^{AD}(\lambda_1) - \frac{Q^D}{Q^A} \cdot \frac{\Gamma_{ex}^{\lambda_1,A}}{\Gamma_{ex}^{\lambda_2,A}} \cdot F^A(\lambda_2)$$

and using the above derivation for  $F^A(\lambda_2)$ ,  $F^D(\lambda_1)$  becomes

$$F^D(\lambda_1) = F^{DA}(\lambda_1) + \frac{Q^D}{Q^A} \cdot F^{AD}(\lambda_1) - \frac{Q^D}{Q^A} \cdot \frac{\Gamma_{ex}^{\lambda_1,A}}{\Gamma_{ex}^{\lambda_2,A}} \cdot \left[ \frac{F^{AD}(\lambda_2) - \frac{\Gamma_{ex}^{\lambda_2,D}}{\Gamma_{ex}^{\lambda_1,D}} \cdot F^{AD}(\lambda_1)}{1 - \frac{\Gamma_{ex}^{\lambda_2,D}}{\Gamma_{ex}^{\lambda_1,D}} \cdot \frac{\Gamma_{ex}^{\lambda_1,A}}{\Gamma_{ex}^{\lambda_2,A}}} \right]$$

Now, we can use  $F^D(\lambda_1)$  to calculate donor concentration from eq. 2.20

$$[D]_T = \frac{F^D(\lambda_1)}{\Gamma_{ex}^{\lambda_1,D} \cdot Q^D} = \frac{F^{D_{only}}(800)}{m_D} \quad (2.29)$$

using  $\lambda_1$  measurement on solution of proteins at known concentration to obtain  $\Gamma_{ex}^{\lambda_1,D}$  and where  $m_D = Slope(D) = \Gamma_{ex}^{\lambda_1,D} \cdot Q^D$  is the slope of the line which is the measurements of intensities at various concentrations of the donor protein solution.

Now, to get the GAR and GDR, an assumption had to be made. The assumption was that you could get excitation rates by looking solely at the  $k^{DA}$  or  $k^{AD}$  images since they are emissions of solutions of donors or acceptors in the presence of the opposite species, which was over a certain duration of acquisition time. Hence, you have a rate of emission, or de-excitation rate. Since we want to see the most common rate of transfer if there was any variation, the average value of  $k^{DA}$  or  $k^{AD}$  was used to calculate GAR or GDR. Therefore:

$$GAR = \frac{\Gamma^{800,A}}{\Gamma^{960,A}} = \frac{Average\ k^{AD}(800)}{Average\ k^{AD}(960)} \quad (2.24)$$

and,

$$GDR = \frac{\Gamma^{800,D}}{\Gamma^{960,D}} = \frac{Average\ k^{DA}(960)}{Average\ k^{DA}(800)} \quad (2.25)$$

These GAR and GDR values were measured on cells transformed with only the acceptor fluorophores or only donor fluorophores to ensure emission was only from one species.

The next step was to convert these total concentrations to molar fractions by simply taking total concentration of one species divided by the sum of the total concentration of both species.

$$X_D = [D]_T / ([D]_T + [A]_T) = \text{molar fraction of donors}$$

and,

$$X_A = [A]_T / ([D]_T + [A]_T) = \text{molar fraction of acceptors}$$

The final step was to calculate the average  $E_{app}$  for the same regions of interest for the same cells. As seen in the above equations, we can get average  $E_{app}$  from

$$E_{app} = 1 - \frac{F^{DA}(800)}{F^{Donly}(800)}$$

These values were calculated and all information was tabulated. Now the data could be graphed as average  $E_{app}$  as a function of molar concentration of acceptors. Once this was done, the sum of both species total concentrations was sorted in ascending order, and ranges were chosen to analyze cells at different expression levels. Ranges of concentrations ( $x$ ) went from  $0 \leq x < 10 \mu\text{M}$ ,  $10 \leq x < 20 \mu\text{M}$ ,  $20 \leq x < 30 \mu\text{M}$ ,  $30 \leq x < 40 \mu\text{M}$ , and lastly  $40 \mu\text{M}$  and above as the last range. When the cells were sorted, the same cells had to stay within the same concentration range from the absence to presence of ligand, or they were discarded due to high variations in the expression levels. Therefore, plotting going further had the same number of cells in each range from the absence to the presence of ligand. For each range, the plot of average  $E_{app}$  versus  $X_A$  was made, and a trendline was added to see if the slopes changed from the absence to the presence of ligand.

## Chapter 3

### THEORETICAL MODELING

#### 3.1. Analysis of $E_{app}$ Histograms

Of the cells co-expressing GFP<sup>2</sup> and YFP tagged Ste2 for the first experiment, the majority of these had narrower  $E_{app}$  histogram peaks positioned along the horizontal axis of the graph (which corresponds to the various  $E_{app}$  efficiencies) with a major or predominant peak (See Chapter 4). These peaks were fitted with a single Gaussian function. Similarly, the slightly more broad histograms (or those displaying a variety of peaks across a wider distribution of  $E_{app}$  efficiencies) that still showed a predominant peak, were also fit with a single Gaussian function. In both cases, the peak position of these predominant peaks were collected and binned to create a “meta-histogram” or a histogram of the various peak positions across all cells in either the ligated or non-ligated case (the data of each was kept separate for analysis). The meta-histogram showed the total number of peak positions of all the cells in one category at an interval of 0.02%. The meta-histograms displayed a variety of peaks and were fit with a dimers only oligomer model. The details of the derivation of this model are given in the next section. The fitting of the simulated Gaussian curves to the experimental data was done by minimizing the mismatch between experimental and simulated data by adjusting the variable parameters of the model.

In this analysis, the exact value of the pair-wise FRET efficiency for a dimer ( $E_d$ ) and the most probable number of donors per pixel ( $n$ ) both determine the position of the various peaks in a histogram and are adjustable parameters.  $E_d$  depends directly on the distance between individual donors and acceptors within the protein complex. This is relative to the Förster radius corresponding to the FRET pair used in this experiment.



The width of the Gaussians in the meta-histograms is not considered of any real significance for this analysis. The factors affecting the width are non-systematical and these include: the orientation of the dipoles, variation of pH, and possible broadening due to mixture between dimers and higher order oligomer structures. These are considered independent parameters and are adjusted independently for the fitting of the meta-histogram.

Next, the amplitudes of the Gaussian curves in the meta-histogram depend on the predominant peak position, so hence it is the number of cells corresponding to a particular  $E_{app}$  value, as well as the total number of cells imaged. This means that we can not necessarily predict amplitudes in a meta-histogram, but rather their peak positions along the  $E_{app}$  distribution. Also, it has been observed that the widths of the individual histograms corresponding to the higher values of  $E_{app}$ , is larger and their amplitudes lower compared to those with lower  $E_{app}$  values, this could lead to missing of some peaks of higher  $E_{app}$  values for the cells, whose histograms showing multiple peaks.

The vast majority of the histograms fell within the narrow category and hence the predominant peaks showed an obvious fit by the dimer model. However, some histograms showed peaks beyond the  $E_d$  value, and these tended to be broader histograms. In this case, these histograms were pulled aside and fit with the dimer model as well and the results are discussed in the Results section.

Since each image contains information about the donor intensities, we use this accompanying data to create a distribution of weighted average of what is known as  $F^D$  only (fluorescence intensity due to donor only). In this case, the weighted average of  $F^D$  only per cell allows for essentially a meta-histogram of  $F^D$  only values to be made. This allowed us to take our analysis one step further to categorize the level of expression based on fluorescence intensity of the donors. The use of this  $F^D$  only value will be further discussed in the Results section as well.

Lastly, the potential for partiality towards the dimer model may occur in the meta-histogram only if there is photo-bleaching or high intensity cells due to high expression. If the intensity gets too high for some complexes, and the mixing tends towards only a certain peak in the histogram, you can have the histogram collapse to a single large, predominant peak. In this experiment, the cells that are too high in expression were very few (approximately 20 cells), and wouldn't have biased the results since these are within range of error. As for the partiality towards the dimer model in meta-histograms, the choice of the maximum peak leads to much overlap below  $E_d$ . Some cells were above  $E_d$ , however, the vast majority of maximum peaks were below  $E_d$ , and the counting of these peaks and binning them lead to many histogram counts below  $E_d$ . This allows for the peaks of the dimer to not be washed out by the broadening of the meta-histogram due to tetrameric oligomers mixing peaks (or smoothing out the meta-histogram). These peaks yield the contour in which the model is fit to, so if the obvious contours above the tetramer mixing (and smoothing out) are that of the dimer, then the dimer model is going to be the obvious best fit. Histogram collapse can be defined as a measured histogram showing one predominant configuration being produced within the cell, so much so that it overwhelms any broadening due to higher oligomerization and creates a dominant peak due to that configuration being produced vastly more than any other. This is noted for this experiment, but since low counts of cells were in this category, the effect appears to be negligible.

### **3.2. Development of the Dimer and Tetramer Models**

#### **3.2.1. Theoretical Modeling of the $E_{app}$ Histograms in Terms of the Dimer Model**

Theodor Förster was a German physical chemist who developed a theory related to a form of non-radiative energy transfer between molecules in 1946. His work has since then been

dramatically developed and the application of the theory of Resonance Energy Transfer (RET) is far reaching. His legacy lives on through the Förster Resonance Energy Transfer (FRET) theory and also the distance at which these interactions occur are also named after him, the Förster radius.

For resonance energy transfer to relate to physical properties of molecules, there must be some physical, measurable quantity from them. For derivations herein, thanks go out to Dr. Valerica Raicu for his expansion of the FRET theory, and the equations themselves [48]. FRET theory starts from simple case of a single energy donor and a single energy acceptor. Starting with the emission rate of photons from the molecules, calculations for the *quantum yield* for both the donor (D) and the acceptor (A) are as follows

$$Q^D = \frac{\Gamma^{r,D}}{\Gamma^{r,D} + \Gamma^{nr,D}} \quad (3.1)$$

and

$$Q^A = \frac{\Gamma^{r,A}}{\Gamma^{r,A} + \Gamma^{nr,A}} \quad (3.2)$$

where  $\Gamma^{r,X}$  and  $\Gamma^{nr,X}$  (for X = D or A) are the rate constants of de-excitation through radiative and non-radiative processes. Also,

$$\frac{1}{(\Gamma^{r,X} + \Gamma^{nr,X})} = \tau_X \quad (3.3)$$

where  $\tau_X$  is the lifetime of an excited molecule X, or a donor or acceptor. Now, say excitation energy can be transferred from donor (D) to acceptor (A). This means an additional pathway exists for de-excitation of molecules. Therefore, the quantum yield is changed to

$$Q^{DA} = \frac{\Gamma^{r,D}}{\Gamma^{r,D} + \Gamma^{nr,D} + \Gamma^{RET}} \quad (3.4)$$

and hence

$$\frac{1}{(\Gamma^{r,X} + \Gamma^{nr,X} + \Gamma^{RET})} = \tau_{DA} \quad (3.5)$$

is the fluorescence lifetime of donor in the presence of an acceptor (otherwise known as FRET).

Now, assume the mechanism of transfer is dipolar, or Förster type, then the rate constant of non-radiative energy transfer from a donor to an acceptor is

$$\Gamma^{FRET} = (\Gamma^{r,D} + \Gamma^{nr,D}) \left( \frac{R_0}{r} \right)^6 \quad (3.6)$$

where  $r$  is the distance between a donor and acceptor, and  $R_0$  is the Förster distance or radius.

Now, RET only takes into account the de-excitation of the donor, but it also effects the excitation of the acceptor and not its quantum yield. This leads to a way to calculate the amount of excitations dissipated through RET by the donor. This term is called RET efficiency and is calculated by

$$E = \frac{\Gamma^{RET}}{\Gamma^{r,D} + \Gamma^{nr,D} + \Gamma^{RET}} \quad (3.7)$$

and assuming  $\tau_{DA} < \tau_D$ , and  $\tau_A$  is unaffected by RET, this equation can be rewritten as

$$E = 1 - \frac{\tau_{DA}}{\tau_D} \quad (3.8)$$

which can also be rewritten as

$$E = \frac{R_0^6}{R_0^6 + r} \quad (3.9)$$

which relates distance between the donor and acceptor to RET efficiency.

From this simple case of one donor and acceptor, we can see how efficiency of non-radiative energy transfer, or resonant energy transfer, can play a large role in understanding interactions between fluorescent molecules.

The rate of energy transfer between a donor and acceptor is given by equation 3.6, where  $R_0$  is the Förster distance,  $\Gamma^r$  is radiative energy transfer rate of donor and  $\Gamma^{nr}$  is nonradiative energy transfer rate for donor and  $r$  is the distance between donor and acceptor. And pairwise FRET efficiency is defined as

$$E_p = \frac{\Gamma^{RET}}{\Gamma^{nr,D} + \Gamma^{r,D} + \Gamma^{RET}} \quad (3.10)$$

or, in terms of Förster distance and the distance between the donor and acceptor,  $E_p$  can be expressed as

$$E_p = \frac{\left(\frac{R_0}{r}\right)^6}{1 + \left(\frac{R_0}{r}\right)^6} \quad (3.11)$$

thus, the apparent FRET efficiency for any complex of acceptor and donor molecules is given by

$$E_{app} = \frac{1}{k} \sum_{i=1}^k E_i \quad (3.12)$$

where  $k$  is number of donors in the complex and  $E_i$  is FRET efficiency for the  $i^{\text{th}}$  donor.

In this case, some particular complexes form purely dimers, that means there are no monomers or higher order oligomers are present. Then,  $E_i$  will be simply equal to  $E_p$  for each FRET productive complex (dimer). The dimers which have only acceptors or only donors, do not FRET, which can be regarded as unproductive FRET pairs. Thus the FRET efficiency for a collection of dimers will be

$$E_{app} = \frac{1}{k} \sum_{i=1}^k E_p \quad (3.13)$$

Intuitively we may want to call  $E_p$  as  $E_d$  for dimers. Thus

$$E_{app} = \frac{1}{k} \sum_{i=1}^k E_d \quad (3.14)$$

### 3.2.2. Probability of Donor and Acceptors, and Calculating $E_{app}$ from Dimer

#### Mixing

Now, let us consider, on average,  $n$  monomers in a pixel of a FRET efficiency map, and all the monomers exist only in dimer form and number of donors is represented by a variable  $k$ , then there will be  $n - k$  acceptors.

If donors ( $D$ ) to acceptors ( $A$ ) concentration ratio is given as  $\rho$ , then the probability of a monomer to be a donor can be expressed in terms of  $\rho$ , as

$$P(D) = \frac{\rho}{1 + \rho} \quad (3.15)$$

and the probability of a monomer to be an acceptor can be written as

$$P(A) = \frac{1}{1 + \rho}. \quad (3.16)$$

Therefore, for  $n$  monomers, the probability that there are  $k$  donors (and thus  $n - k$  acceptors) is given assuming a binomial distribution:

$$P(n, k) = \binom{n}{k} P(D)^k P(A)^{n-k} \quad (3.17)$$

We then derived a general mathematical expression for the FRET efficiencies ( $E_{app}$ ) for any  $n$  and  $k$ . The expression is give as

$$Series(E_{app}) = \frac{1}{k} \sum_{k=1}^{n-1} \sum_{i=0}^{i < \frac{d}{2}} \frac{(d - 2i)}{k} E_d \quad (3.18)$$

where  $d = \min(k, n - k)$

Now, consider a Gaussian with peak (mean positions) as  $E_{app}$  and its amplitude is proportional to a general expression for probability for their being  $k$  donors out of  $n$  monomers, which depends on donors to acceptors concentration ratio  $\rho$ . Then a function, which is the sum of all these Gaussians for variables as numbers of monomers ( $n$ ), pairwise FRET efficiency for the dimer (which depends on the distance between donors and acceptor and Förster distance for the fluorphores pair)  $E_d$ , and donors to acceptors concentration ratio  $\rho$  and standard deviation  $\sigma$ , is given as

$$f(E_{app}) = \frac{1}{k} \sum_{k=1}^{n-1} \sum_{i=0}^{i < \frac{d}{2}} \frac{(d - 2i)}{k} E_d A(n, \rho) \sigma \quad (3.19)$$

where  $A(n, \rho)$  is the amplitude of a Gaussian and is given by

$$A(n, \rho) = \text{Const.} \binom{n}{k} P(D)^k P(A)^{n-k} \quad (3.20)$$

where *Const.* is a proportionality constant. So, if one has an experimental histogram for the complexes which have only dimeric form, then the histogram can be fitted with this model (or the function *f*) and *n*, *σ* and *E<sub>d</sub>* and the *Const.* can be used as fitting parameters.

### 3.2.3 Theoretical Modeling of FRET efficiencies in the Parallelogram-Shaped Tetramer

If *r<sub>1</sub>* and *r<sub>2</sub>* are the two sides of the parallelogram and *α* is the angle between the two sides of the parallelogram then the diagonal *r<sub>d1</sub>* is given by

$$r_{d1} = (r_1^2 + r_2^2 - 2r_1r_2 \cos \alpha)^{1/2} \quad (3.21)$$

Also the pairwise FRET efficiency between *i* = 1 and *j* = 1 is given by

$$E_1 = \frac{\left(\frac{R_0}{r_1}\right)^6}{1 + \left(\frac{R_0}{r_1}\right)^6} \quad (3.22)$$

and from Eq. (3.22)

$$\left(\frac{R_0}{r_1}\right)^6 = \frac{E_1}{1 - E_1} \quad (3.23)$$

and thus

$$\left(\frac{R_0}{r_k}\right)^6 = \frac{E_1}{1 - E_1} \left(\frac{r_1}{r_k}\right)^6 \quad (3.24)$$

where *k* can take two values, *d1* and *d2*.



Now, the apparent FRET efficiency for the configuration shown in the Figure 3.2 below is given by

$$\frac{E_{app}}{E_{app} + 1} = \frac{r_1^6 + r_2^6}{r_1^6 + r_2^6 + r_{d1}^6 + r_{d2}^6} \quad (3.25)$$

recognizing  $r_1$  as  $r_1$  and using equation (3.22)

$$\frac{E_{app}}{E_{app} + 1} = \frac{r_1^6 + r_2^6}{r_1^6 + r_2^6 + r_{d1}^6 + r_{d2}^6} \quad (3.26)$$

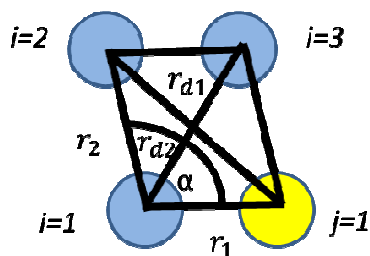


**Figure 3.2.** Parallelogram-shaped tetramer geometry. The various fitting parameters are displayed as  $r_1$  and  $r_2$ , or the distances between two protomers in a tetramer depending on the side chosen,  $r_{d1}$  and  $r_{d2}$  are the diagonal distances between opposite sides of a parallelogram configuration, lastly  $\alpha$  is the angle between two sides of a parallelogram. These fitting parameters are used to change the location of the various peaks in a meta-histogram along the  $E_{app}$ -axis allowing for a theoretical model of the tetramer to be applied to experimental data.

One configuration of a parallelogram-shaped tetramer model is represented by three donors and one acceptor as seen in Figure 3.2. Then  $r_1$  and  $r_2$  represent the two sides of the parallelogram,  $\alpha$  is the angle between two side of the parallelogram,  $r_{d1}$  and  $r_{d2}$  are the two diagonals of the parallelogram. Here  $r_1$  represents the donors while  $r_2$  the acceptors.  $r_{d1}$  is short diagonal distance while  $r_{d2}$  is the long diagonal distance.

Similarly,

$$\frac{-}{\frac{-}{-} \quad \frac{-}{-} \quad \frac{-}{-}}$$

(3.27)

and plugging equations (3.26) and (3.27) in equation (3.25), we get

$$\frac{-}{\frac{-}{-} \quad \frac{-}{-} \quad \frac{-}{-}}$$

(3.28)


and hence

$$\frac{-}{\frac{-}{-} \quad \frac{-}{-} \quad \frac{-}{-}}$$

(3.29)

is the expression for apparent FRET efficiency in terms of the sides of the parallelogram, the diagonals and pairwise FRET efficiency. Similarly the FRET efficiency expressions for the other six possible configurations can be derived and their expressions are tabulated in the table below.

**Table 3.1.** Eapp peaks predicted by the parallelogram tetramer model and their corresponding configuration of protomers

| Peak Number |   | Configurations  |
|-------------|---|---|
|             | $\frac{-}{\frac{-}{-} \quad \frac{-}{-} \quad \frac{-}{-}}$ |  |

|  |  |  |
|--|--|--|
|  |  |  |
|  |  |  |
|  |  |  |
|  |  |  |
|  |  |  |
|  |  |  |

## Chapter 4

### RESULTS AND DISCUSSION

#### 4.1. Refining the Quaternary Structure of Ste2

##### 4.1.1. Determination of the smallest oligomer size

To probe the oligomerization of the Ste2 receptors in living cells along the cellular surface, or plasma membrane, we employed an optical micro-spectroscopic (OptiMiS) technique described in Chapter 2 and FRET to quantify the interactions of the receptors as described in previous publications [33, 35, 47, 49]. To determine the FRET efficiencies, we first induced yeast cells to express only the Ste2-GFP<sub>2</sub> (i.e. the energy donor) or only the Ste2-YFP (i.e. the energy acceptor). By imaging cells we determined the elementary spectra of the donor and acceptor tags, which were subsequently used for un-mixing each image of cells co-expressing the two fluorescent species.

Next, the cells that are co-expressing GFP<sub>2</sub> and YFP at a one-to-one (1:1) ratio of each fluorescent tag on the Ste2 receptors (as quantified by the amount of DNA used) were imaged. Images were acquired using OptiMiS imaging system [46] and two dimensional maps of the donor fluorescence intensity in the presence of acceptors ( $k^{DA}$ ) and acceptor fluorescence intensity in the presence of donors ( $k^{AD}$ ) were obtained using spectral unmixing (see Chapter 2.5, 2.6) [22]. Spatial distribution maps of apparent FRET efficiencies ( $E_{app}$ ) were computed based off of the  $k^{DA}$  and the  $k^{AD}$  values at each image pixel using mathematical equations derived previously [22]. Figure 1 shows typical results of the  $k^{DA}$  and the  $k^{AD}$  images of a representative cell co-expressing GFP<sub>2</sub> and YFP and the resultant  $E_{app}$  map as described in Chapter 2.6.3. Also seen in Figure 1 is the  $E_{app}$  histogram that was generated by binning the  $E_{app}$  image pixels

according to their value (in this case, bin size 0.01) and plotting their number of pixels in each bin against  $E_{app}$ .

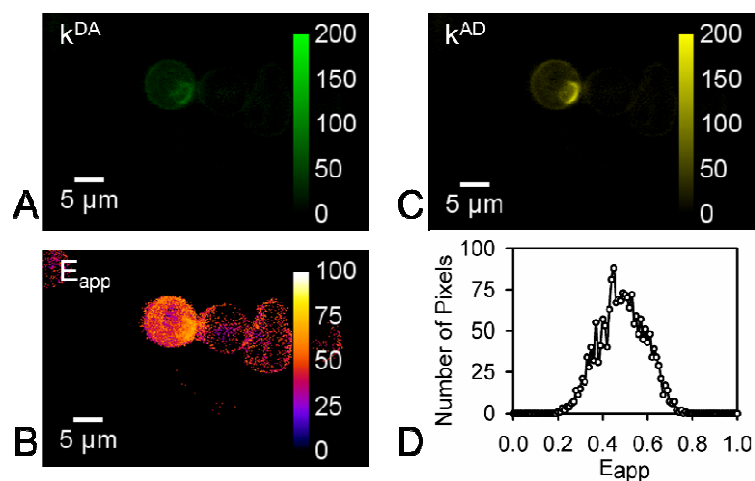


**Figure 4.1.** Typical FRET results of *Saccharomyces cerevisiae* expressing Ste2p fused to GFP<sub>2</sub> and, separately, YFP. Spectral un-mixing of spectrally resolved fluorescence micrographs resulted in spatial distributions of donor emission in the presence of acceptors (A) and acceptor emission in the presence of donors (B). A two-dimensional spatial distribution map of apparent FRET efficiencies ( $E_{app}$ ) was obtained from pixel-level calculations based on the data in panels A and B as described in the methods section (C). The two-D  $E_{app}$  map shown in panel C was used to compute an  $E_{app}$  distribution by binning and plotting histograms the FRET efficiencies, in a bin interval of 0.02. Scale bars used in all images, 5  $\mu$ m.

Previously, it has been reported that collecting positions of the dominant peaks as seen in Figure 4.1D, and plotting the number of peaks whose positions fall within a certain range of  $E_{app}$  values against the  $E_{app}$  value a *meta-histogram* of FRET efficiencies is obtained [33]. This meta-histogram allows for the isolation of signal corresponding to dimers from a background count of higher order oligomers [40]. The co-localization within a single pixel of monomers, dimers, and higher-order oligomers leads to the combination of their signals which give a variety of peaks in the original histograms that are larger than the highest order structure present. Realizing that oligomers composed only of acceptors are not considered, due to the laser negligibly exciting these in this experiment, is crucial to understanding the ability to mix various proportions of donors and acceptors at each pixel.

To explain this mixing further, consider if six configurations corresponding to the rhombus-shaped tetramer and containing donors shown in Figure 4.1A are combined two at a

time, on average, at each image pixel, the number of new peaks is twenty, and it increases dramatically if more than three tetramers combine at each pixel. When large numbers of peaks combine, eventually a broad background in the met-histogram occurs, washing out any indication of the structures present, in combination with the numbers of cells imaged in this experiment (~1000 cells total) and the bin size of the typical histogram of 0.01 or 0.02.

Next, to contrast this previous argument, consider that for dimers at relatively high expression levels, the number of peaks resulting from the combination of dimers at each pixel may still be small enough to allow individual peaks to be resolved within the *meta-histogram*. Figure 4.2B shows that if you combine two dimers, then only two peaks will form, however the second dimer, is composed only of non-FRET producing donors. When averaging three, or four dimers per pixel, the number of peaks that occurs is simply three or four, or so forth. This leads to the idea that large numbers of dimers per pixel still may be able to be resolved. Due to the non-uniform distribution of the number of dimers per pixel (see Figure 4.2C), some peaks should be larger than others within the *meta-histogram*, but still much lower than that expected for tetramers.

Lastly, a mixture of dimers and rhombus shaped tetramers at each pixel would yield broad *meta-histograms* with poorly resolved backgrounds. This is due to the combination of tetramers, as well as the combination of tetramers and dimers, which are both described above. However, in the mixture of tetramers and dimers, the broad background has peaks that “shine” through due to the combinations of dimers. When attempting to analyze the meta-histogram, theoretical Gaussian peaks are only used to simulate the peaks corresponding to the combination of dimers (as seen in figure 4.2C). The broader background due to the tetramers is captured by the width of each of these Gaussians, and their overlap.

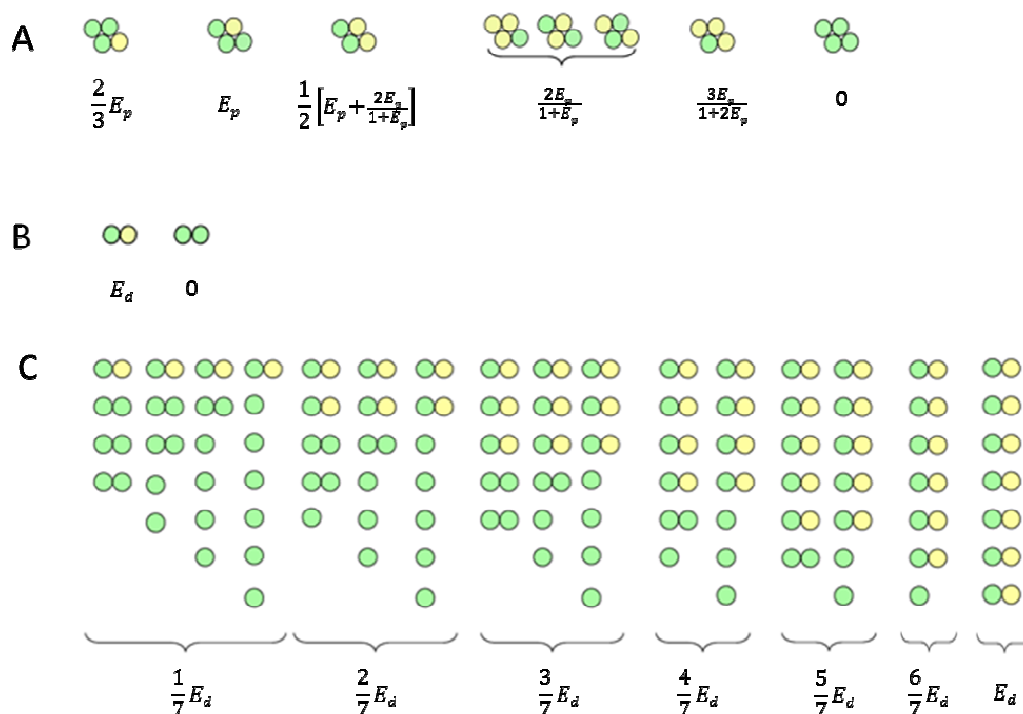


**Figure 4.2.** Donor-acceptor configurations and their respective peak positions for rhombus-shaped tetramers (a) and dimers (b) at low expression levels, as well as for a mixture of DD and DA dimers at high expression levels (c).

Figure 4.2 depicts the first two models that apply to a system of proteins at low expression levels. For higher expression levels, both the dimer and tetramer predict larger numbers of peaks compared to when only a single complex lies on a single pixel. The figure only provides the expressions for single tetramers, as the schematic becomes too large to represent. For combinations thereof dimers, in 4.2C, we can see that the combination of up to eight donors (composed of donor-acceptor, or donor-donor dimers) residing at each pixel, can yield up to eight combinations of dimers (donor-donor- and donor-acceptor dimers). For larger numbers of donors per pixel, the number of predicted meta-histogram peaks increases, eventually surpassing the resolution of the experiment (i.e. the bin size of the histogram).

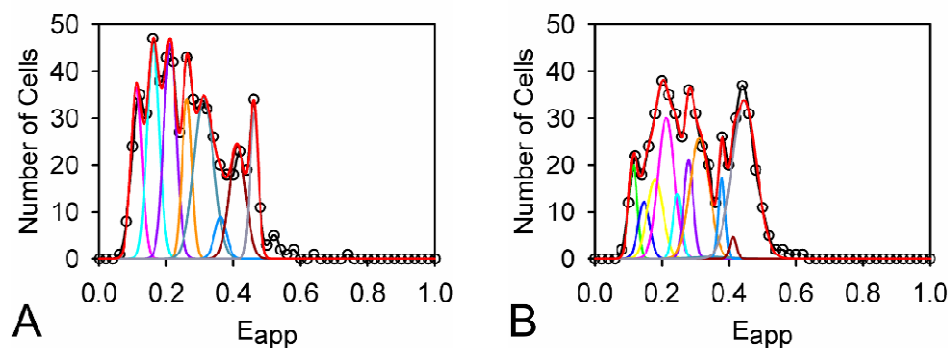


**Figure 4.3.** Meta-histograms of FRET efficiencies obtained from images of cells in the absence (A) and in the presence (B) of the  $\alpha$ -factor pheromone. The red line indicates the theoretical fit, empty circles represent the experimental data, and the other individual lines represent the various peaks of theoretical Gaussians defined by the dimer model in Chapter 3.2.1 and 3.2.2.

For the Ste2 receptor in the presence and absence of the natural ligand, alpha-factor, the *meta-histograms* are presented in Figure 4.3. When attempting to theoretically fit these to the model described above, composed of dimers and tetramers, the solid red line was obtained, which in both the presence and absence of the ligand capture the significant features of the experimental data. The fitting parameters that determines the position of all the peaks was the  $E_{app}$  value that corresponds to only donor-acceptor pairs (or dimers). This values is called pairwise FRET efficiency, labeled by  $E_d$ , which is the same as the first column found in figure 2c. The average number of donors per pixel, which can take non-integer values, due to being an average from more than one cell comes from the inhomogeneity in expression across all cells. The widths and amplitudes of the theoretical Gaussian functions are not predicted by the theory, hence these values are not given or described herein. As for the peak corresponding to  $E_d$ , its position in the *meta-histogram* is right-most, while all other peaks are laid out from right to left in order of decreasing numbers of donor-acceptor pairs. These peaks originate from the different proportions of the donor-donor and donor-acceptor pairs.

The result of the meta-histogram analysis revealed that the monomeric donors did not have to be considered to fit the experimental data. If there was an obvious presence of these



monomers, the *meta-histogram* would have yielded additional peaks. If free donors were available, Figure 2c would have one of the five donors in the first column to be only a monomeric donor, and the other five would have been donor-acceptor dimers. In this case, there would have been an additional peak that was seen which would reside at  $4/5E_d$  within the *meta-histogram*.

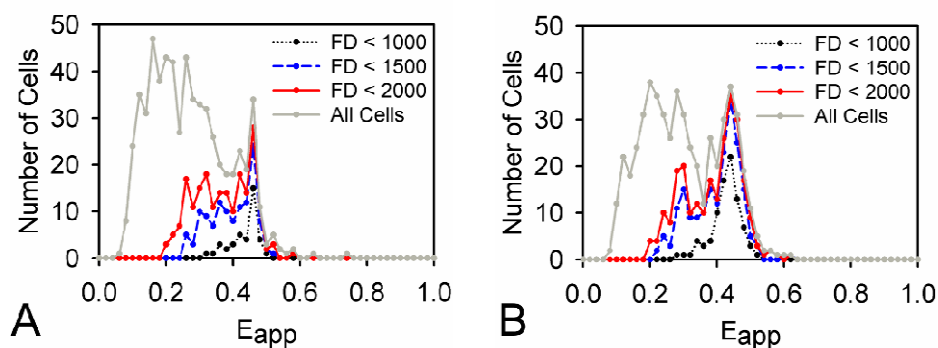


**Figure 4.4.**  $E_{app}$  meta-histograms for three different expression levels of donors in the absence (A) and presence (B) of alpha factor ligand. The ranges of donor concentration per cell, in arbitrary units, are listed in the legends. Donor concentration was estimated in terms of the average donor fluorescence corrected for FRET ( $F^D$ ) according to the formula:  $F^D = F_{obs} / (1 - FRET)$ , which may be obtained readily from the theory presented in Chapter 2.6.3 and 2.7[5].

#### 4.1.2. Probing for higher order oligomers

Previous publications from our lab suggested that rhombus-shaped tetramers must be present [5], therefore it can be stated that the dimers found within the meta-histogram can also associate to form tetramers, and revert back to dimers, but not monomers. We therefore wanted to confirm that result. The next step in the analysis was to examine the average value of donor fluorescence for each cell, when corrected for FRET. This value is called  $F^D$ , and each cell was averaged over its area and categorized based upon it. The categorization was to look at the three lowest ranges of FD (in arbitrary units). These ranges were 0 to 999, 1000 to 1499, and 1500 to 2000. The lowest level of signal determined from spectral unmixing revealed that the we must consider counts above a few tens of arbitrary intensity counts to account for noise

levels, which varied for cell to cell. Seen in Figure 3a and b, the decreasing expression levels of donors yields a disappearance of the peaks left of  $E_d$ . If the dimers truly dissociate in the process, the peak corresponding to  $E_d$  should also have disappeared, which is not the case. This shows a stable dimeric structure that is similar to other results found on the M3 muscarinic receptor [36], but it also indicates that the dimers are associated to form higher order oligomers, such as tetramers.

The histograms gathered from both the non-ligated and ligated portions of the experiment yielded a variety of shapes. However, most of the histograms contained a single obvious predominant peak. These were the peaks measured and counted for the meta-histograms displayed in figure 4.4A and B. But a variety of histograms at every expression level still led to a variety of questions about higher order oligomerization. Figure 4.5A and B shows a series of histograms at various expression levels and for non-ligated and ligated cells as well. In both cases, there are broad histograms, and narrow histograms. As the expression level was lowered, broader histograms were counted more often. At the same time, it was noticed that some histograms had various peaks located beyond that of  $E_d$  as indicated by the red line in the graphs in Figure 4.5. The red line represents the peak location of the last theoretical Gaussian curve or  $E_d$  for both the non-ligated and ligated cases, and was determined using the application of the dimer model on the meta-histogram.  $E_d$  was measured to be located centered at 0.46 or 46% for the non-ligated cells, and 0.44 or 44% for the ligated cells. The top two cells in Figure 4.5 for both non-ligated and ligated cases show broader histograms with actual measured peaks beyond  $E_d$ .

This led to defining the criteria for determining if a histogram is broad or narrow. A narrow peak must be single very obviously single peaked, and its location must fall below the  $E_d$  value. These narrow peaks must be lower than 0.20 or 20% in width at full-width at half-

maximum value of the measured predominant peak. Then broad histograms must contain all the cells that are not within those guidelines, or histograms that sometimes contained more than one predominant peak, and wider than 0.20 or 20% along the  $E_{app}$  scale. However, it was seen within the broad histograms described above in Figure 4.4, that some were broad and had peaks located beyond  $E_d$ . Hence, a subcategory of broad histograms had to be created. The result was breaking broad histograms into those that showed peaks only measured below  $E_d$  and those that showed measured peaks beyond  $E_d$ .

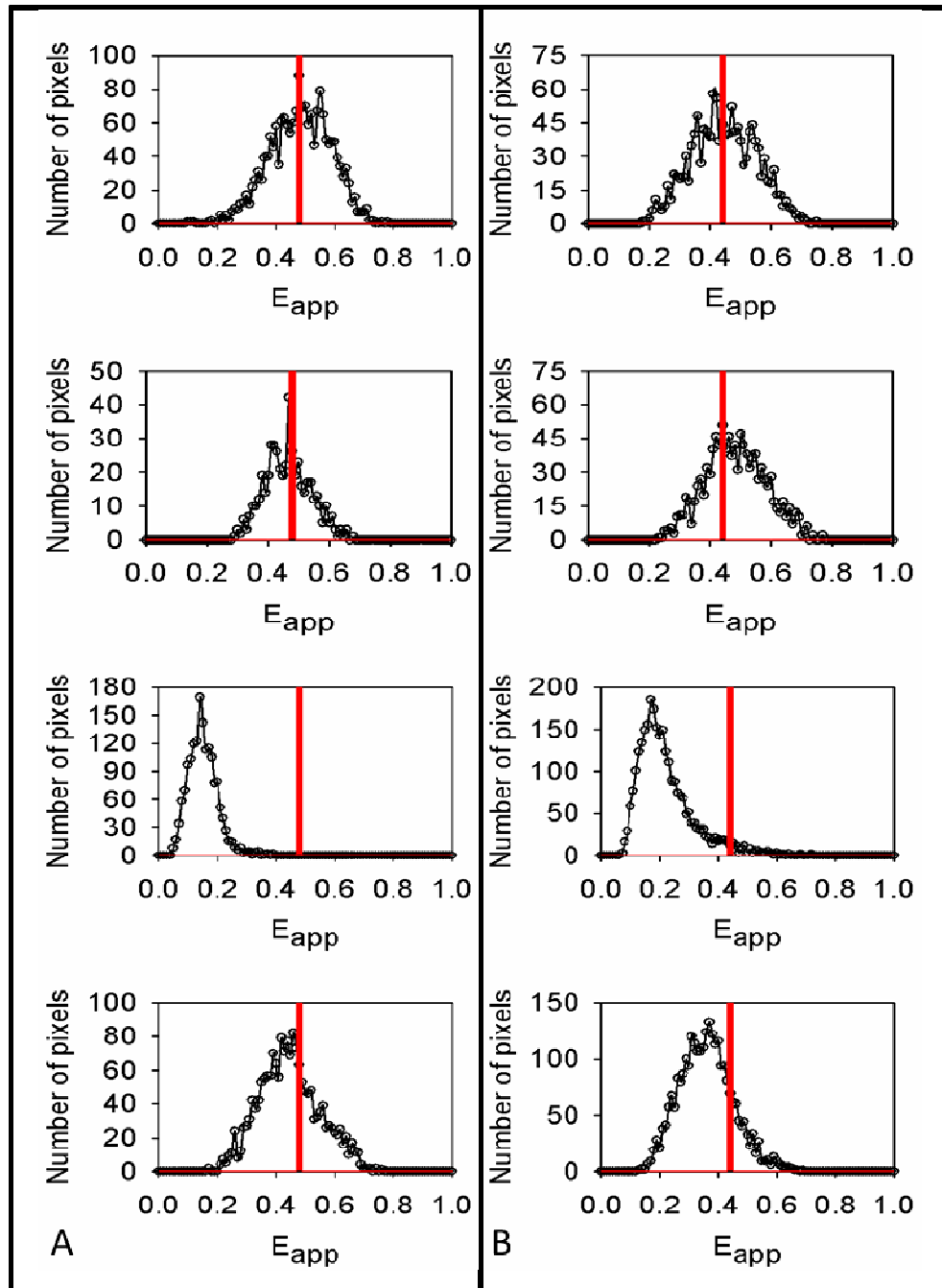


**Figure 4.5.** Examples of histograms (out of a total of 39 cells untreated and 87 treated cells) presenting features at, below, or above  $E_d$ . A) Yeast cells not treated with alpha factor. B) Yeast cells treated with alpha factor. For some of these histograms, it is clear that  $E_d$  would need to be shifted higher to fit all of the peaks. Note that a model composed only of dimers will not capture these peaks beyond  $E_d$ .

Figure 5 shows a variety of histograms for both non-ligated and ligated cells at various expression levels that have real peaks beyond  $E_d$ . If there are peaks beyond  $E_d$ , this means there must be some other complexes than just dimers since the  $E_d$  peak of the dimer model is the

furthest most peak for the dimer model. Hence, to examine if there were some higher order oligomerization in these histograms, a tetramer model (described in the Materials in Methods section) was used to test if  $E_p$  could be set near the  $E_d$  value to see if the theoretical peaks of the model would line up closely with those measured peaks beyond  $E_d$ . Also, having compared a variety of models such as a mixture of free monomers and dimers, a tetramer alone (rhombus, and parallelogram), and the mixture of parallelogram with dimers, the parallelogram with dimers model yielded the lowest residual fit between the theoretical model and experimental data. Figure 4.6 uses the seven peak parallelogram model previously described in the Chapter 2, as well as the two ways a dimer can split, horizontally or vertically. Only six of the theoretical peaks are used to do the fitting in the parallelogram model, because two of the peaks in this model tend to overlap almost identically. Thus, eight theoretical Gaussian peaks are used to generate the model seen in Figure 4.6. The result is an obvious higher oligomerization for the broad histograms at various expression levels that have peaks measured beyond  $E_d$ , as well as a common predominant peak at  $E_d$ . This peak at  $E_d$  is amplified by the mixture of pairwise FRET efficiency of the tetramer, or  $E_p$ , and the  $E_d$  of the dimer. The validity of using single tetramers and dimers per pixel as opposed to the dimer model which takes into account large numbers of molecules per pixel is in the fact that the histograms used in Figure 4.6 are of such low  $F^D$  intensity, that using concentration calibration<sup>14</sup>, we can see that these are near the order of single molecule per pixel expression levels. None of the histograms in Figure 6 are above 1200  $F^D$  only counts. The calibration of GFP<sub>2</sub> yielded 120 counts of photons per pixel using this system configuration. Comparing the data, we can see that if you add the intensity given from a tetramer and dimer together, one can arrive at a number near the limiting value of these histograms in Figure 4.6. Not only does the dimer fall exactly at  $E_d$  and  $E_p$ , but the tetramer peaks yielded the lowest residual fitting value and this tells us that there is obviously some

higher order oligomerization mixed with the dimer being the lowest order stable configuration. However, at this stage it was definitively unclear what the higher order oligomer was, and if there was any effect due to the ligand.

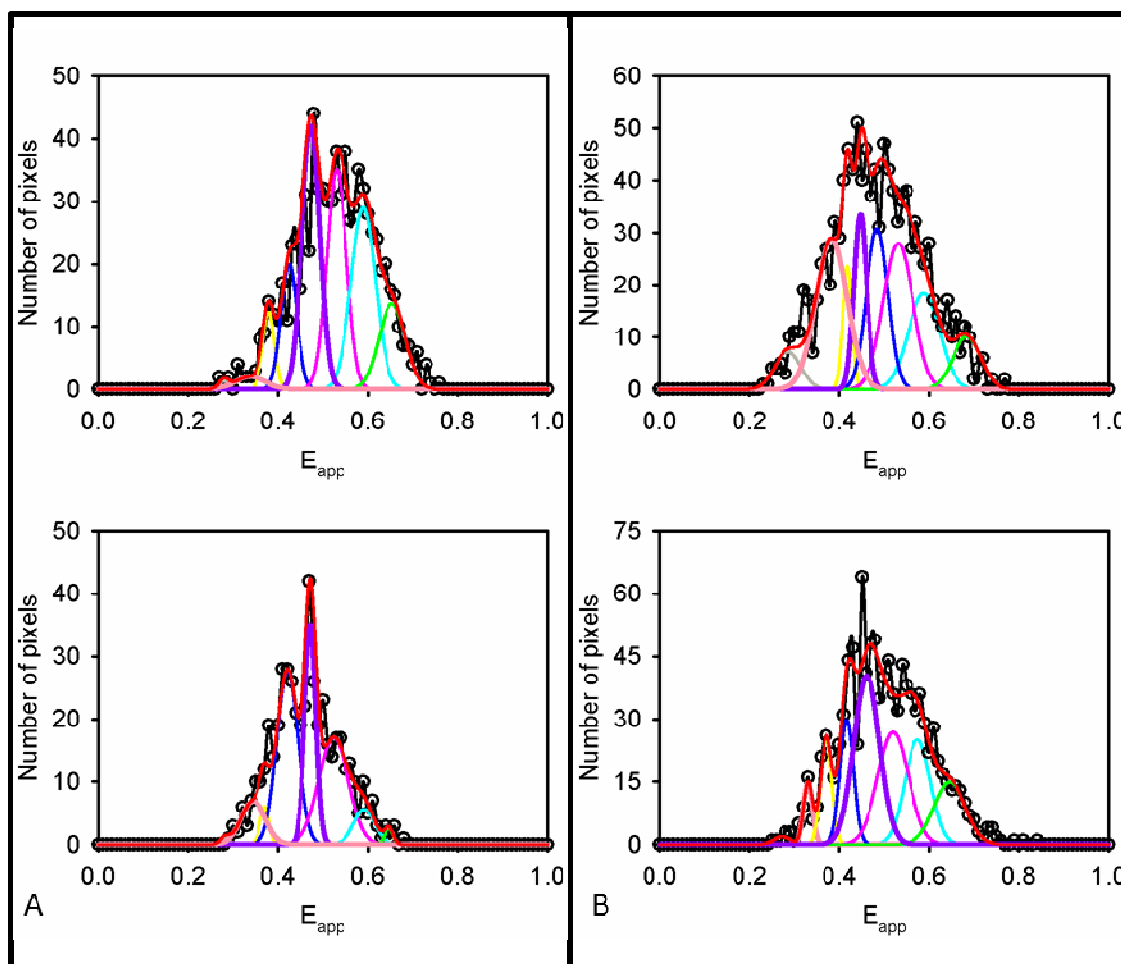


**Figure 4.6.** Representative histograms of cells that fall within the lowest range of  $F^D$  only and have measured peaks beyond the  $E_d$  value for both the absence (A) and presence (B) of the alpha factor ligand.

#### 4.1.3. Distribution of Apparent FRET Efficiencies

Since each cell represents a number of pixels on the camera, and each pixel is able to calculate  $E_{app}$  values, a distribution of efficiencies of FRET for the selected cell can be established. By counting how many cells are at each level of efficiency within the distribution, we would establish what is called an “ $E_{app}$  histogram” by plotting the count of pixels at each efficiency

between zero to one-hundred percent. Since biology allows for vast variability, there is a variety of forms the histograms can take, namely narrow mostly single-peaked histograms to broad, many-peaked histograms. Also, the number of pixels counted for these cells can vary depending on their expression of the two tagged fluorophores. Cells showing lower intensities than the chosen 1.0% threshold of signal to noise were rejected for analysis, as these may provide false FRET readings if the signal was confused for background noise collected by the camera. Once all of the histograms were filtered through this scrutiny, further analysis of the histograms was performed.

## ***4.2. Assessing the Effect of Ligand on Populations of Dimers and Tetramers***

### ***4.2.1. Determination of Concentrations of Ste2 Receptors in Living Cells through Calibration via Fluorescent Protein Solution Measurements***

To estimate protein/receptor concentrations within living cells, protein solutions were developed and synthesized by Lucigen (Middleton, WI, U.S.A.) to mimic the identical proteins tagged to the Ste2 protein within the living yeast cells. These protein solutions were given to us at 4.5 mg/mL for GFP<sub>2</sub>, and 3.5 mg/mL for YFP. The stock molar concentration was found to be 166.697 μM for GFP<sub>2</sub> and 129.6532 μM for YFP. Using these values, and the equation for desired concentration,  $n_i v_i = n_f v_f$ , where  $n_i$  is the initial molar concentration,  $v_i$  is the required volume of the solution to make the desired concentration,  $n_f$  is the desired concentration, and  $v_f$  is the desired volume. By subtracting  $v_i$  from  $v_f$ , the required amount of Phosphate Buffer Solution (PBS) could be calculated to create the desired concentration. Both stock solutions were then reduced in to various concentrations for measurement at their excitation maxima. The estimated concentrations used for imaging both GFP<sub>2</sub> and YFP were 2.5 μM, 5.0 μM, 10.0

$\mu\text{M}$ ,  $20.0\mu\text{M}$ , and  $40.0\mu\text{M}$ . A chambered slide was used to ensure a uniform layer of solution to be excited and measured.

Initial measurements found that the charge on the chambered slide would attract deposits of GFP<sub>2</sub> and YFP and form clumps which would give irregular and inconsistent measurements. To counter this effect, pre-loading slides with Bovine Serum Albumin (BSA) would allow those excess charges to be neutralized and hence make a stable suspension of protein solution. The protocol for coating a slide with BSA was to first make a 1% BSA solution in PBS. Then 200  $\mu\text{L}$  of BSA+PBS solution were added to 10 chambers of the chambered slide. The slide was then incubated at 37° C for one hour and then the solution was removed from the slide. The slide was then filled with 200  $\mu\text{L}$  of PBS to ensure viability of the deposited BSA for the experiment. The slide was then covered and taken to the imaging facility and each chamber had the PBS removed before the protein solution was added for imaging. BSA was found to have negligible auto-fluorescence, and a variety of control experiments were done to ensure negligible effects of measuring protein solutions spectra with pre-loaded slides. Control experiments included: measuring PBS in a coated versus uncoated slide, measuring protein solutions in coated versus uncoated slides, measuring protein solutions in a mixture with BSA to create a solution of both on a coated and uncoated slide, and lastly, measuring auto-fluorescence of a coated versus an uncoated slide alone.

After these control experiments were performed, the use of the coated slide was approved to do measurements on the various concentrations of protein solutions. The solutions were made within a dark room with only yellow light that does not excite the proteins of interest. Each desired concentration was measured using pipettes and both vortex spun and sonicated to ensure no association into larger clumps. After proper mixing, 200  $\mu\text{L}$  of the protein solution at a single concentration was added to the chambered slide coated with BSA.



The solution was imaged numerous times (8 images per concentration) in a variety of fields of view to ensure repeated results. After these measurements were taken, the solution was removed from the slide without touching the BSA coating, and was saved in a 1.5 mL flask and covered with aluminum foil to avoid excitation and photobleaching. After each concentration of GFP<sub>2</sub> and YFP was measured, all the saved flasks were taken to be measured on a spectrophotometer (DU-800, Beckman Coulter, Brea, CA, U.S.A.) to measure absorption and using the Beer-Lambert Law, find the exact concentration of the solutions. The spectrophotometer would scan from 800 nm to 200 nm and to check the DNA absorption the plotted graph of absorption versus wavelength would give the proper measurement at 280 nm. The Beer-Lambert Law states that

$$a = c \epsilon l,$$

where  $a$  is the absorption,  $c$  is the concentration,  $\epsilon$  is the extinction coefficient of the protein of interest, and  $l$  is the path length. Since the path length was standardized to 1 cm, the equation could be rewritten to solve for concentration. Therefore,  $c = a/\epsilon$ , and hence a near exact calculation of concentration could be made. Since you are solving for  $c$ , and  $a$  is given,  $\epsilon$  must be known as well.  $\epsilon$  was found by using the DNA gene sequence for either GFP<sub>2</sub> or YFP given from Lucigen, and placing that sequence into ExPASyProtParam Tool yields various physical parameters, including the extinction coefficient. ProtParam Tool gives two ranges of certainty in their calculations, and the higher of the two was always chosen. Using these estimated values, the concentrations for each flask of an estimated concentration was calculated.

Afterwards, the raw data taken during imaging was then processed in ImageJ software and a region of interest was taken for each image (and was kept the same size and location throughout) to create a histogram of the number of counts per each of the 200 wavelengths. The lowest number of counts per each image was subtracted from each measurement taken at

each wavelength to remove background levels of noise. Once subtracted, the values were summed and hence yielded either  $F^D$  only for GFP<sub>2</sub> or  $F^A$  only for YFP according to eq. 2.18 and 2.20. The sums were taken from each image and averaged for each concentration. The slope was measured by a trendline and used in the calculation of total concentration and molar concentration of proteins within living cells as found in Chapter 2.7. The slope of GFP<sub>2</sub> was found to be 1350.2 and the slope of YFP was found to be 1369.7, as seen in Figures 4.7 and 4.8.

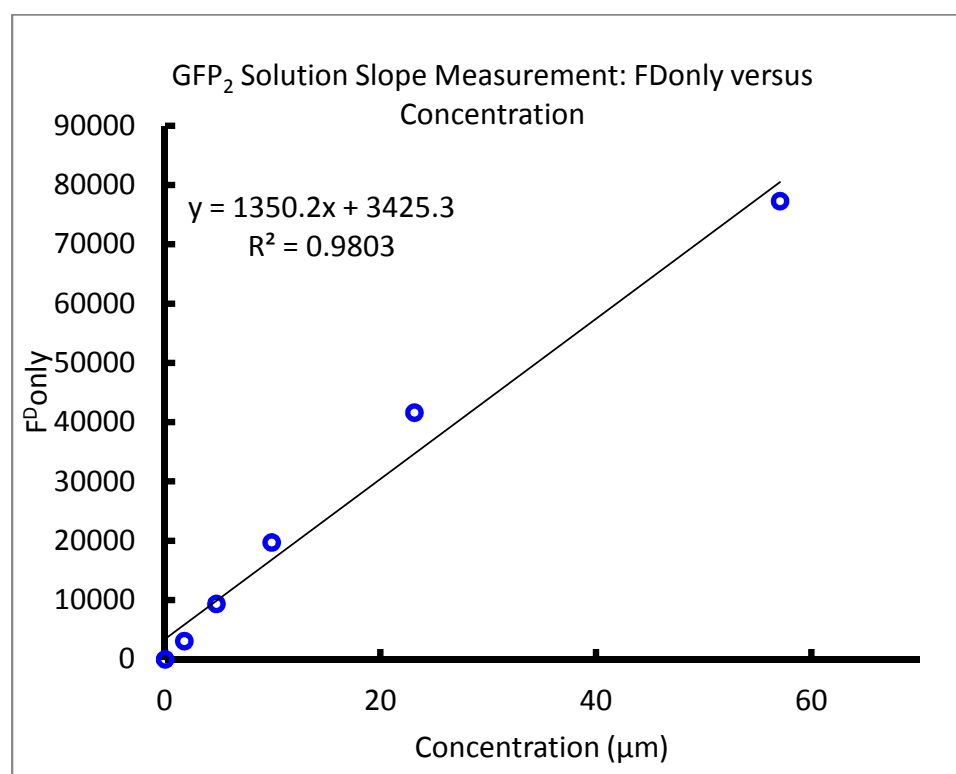


**Figure 4.7.** Slope of GFP<sub>2</sub> protein solution at various concentrations and their corresponding arbitrary intensity counts. Each point on the graph corresponds to an average over eight separate measurements of the same sample.

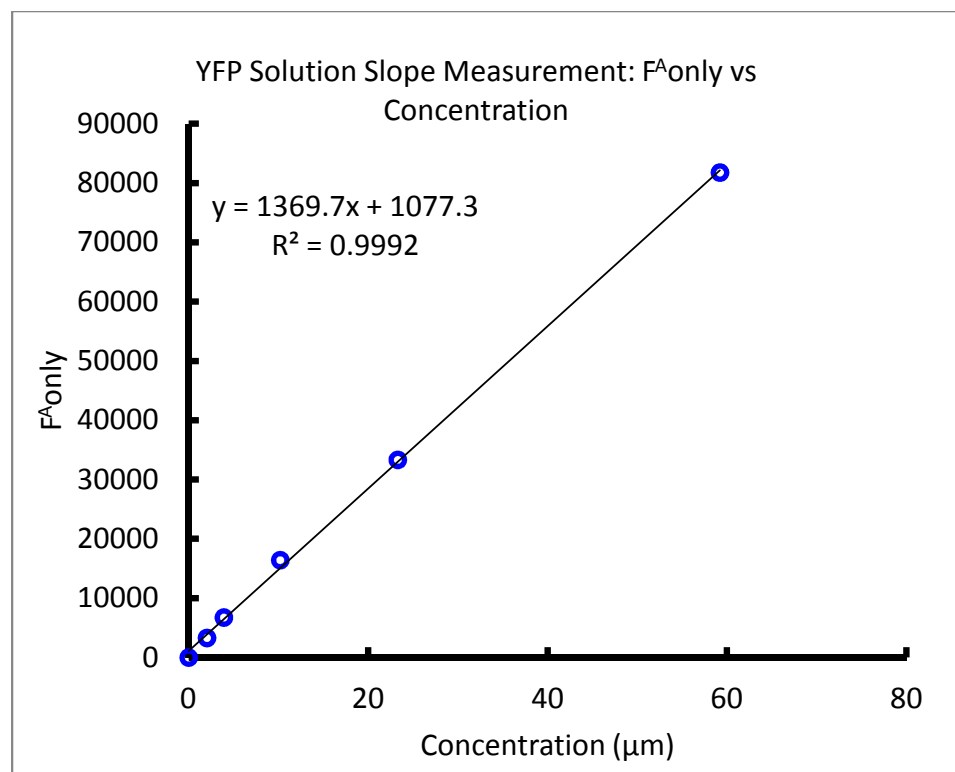


**Figure 4.8.** Slope of YFP protein solution at various concentrations and their corresponding arbitrary intensity counts. Each point on the graph corresponds to an average over eight separate measurements of the same sample.

#### 4.2.2. FRET Efficiency vs. Concentration of Ste2 Receptors in the Presence and Absence of Ligand

In the subsequent experiment involving two wavelength excitation and imaging of cells in the presence and absence of the  $\alpha$ -factor ligand, the system settings were as follows:

1. 800 nm @ 300 mW, Line dwell time of 35 ms, Spectral Resolution 1
2. 960 nm @ 300 mW, Line dwell time of 35 ms, Spectral Resolution 1

Both wavelength images had a 440x200 pixel size, and 200 wavelengths per pixel. The sequence of imaging always went from 800 nm to 960 nm before the introduction of ligand, and then 800 nm to 960 nm after the introduction of ligand. Retaining similar laser power settings allowed for the analysis of two wavelength excitation described in Chapter 2.7. The cells were placed on a

dish, ligand was introduced and then the same cells were imaged. Once finished, the cells and dish were discarded, and the process was repeated until the experiment was concluded.

In both the presence and absence of the ligand, it is now known that both dimers and higher order oligomers are present. To further explore if the ligand has an effect on association, we departed from the meta-histogram method to look at average  $E_{app}$  plotted against molar concentration of the acceptor. First, images were taken of the same cell before and after introduction of the ligand by immobilizing the cells with Concanavalin A. Concanavalin A binds specifically yeast cell vacuoles and plasmalemma, and having been deposited on the imaging dish lead to cells being bound to the dish. Having immobilized cells allowed for imaging before and after introduction of ligand at two wavelengths. Both the donor excitation maxima (800nm) and the acceptor excitation maxima (960nm) were used in both cases, with equivalent laser powers (300mW). After imaging, the cells were spectrally unmixed by only selecting a region of interest which indicated the cellular membrane where the Ste2 receptor is found in its functional form. Similar to Figure 4.1, images containing information pertaining to the  $k^{DA}$  and  $k^{AD}$  at both wavelengths, before and after ligand were obtained. Using the same region of interest for each 800nm and 960nm, before and after introduction of ligand image to ensure averaging areas were unchanged. The  $k^{DA}$  and  $k^{AD}$  information was then processed to gather the average concentrations of donors and acceptors present in each cell, which lead to determining the molar concentration of each. Also calculated from this data was the average  $E_{app}$  value for the cells. This allowed for the plotting the average  $E_{app}$  value of each cell in the experiment before and after introduction of the ligand as a function of its molar concentration of acceptors. The result was a plot that applies a linear trend line to all the cells in each category. This plot displays an obvious slope difference between absence and presence of ligand. The slope difference becomes obvious when looking at the overall percentage change between a control

experiment, where the same protocol was used on the cells for imaging and preparation, only to not administer the ligand. This experiment shows that if you do not introduce the ligand, that the cells remain nearly identical when imaged twice. A slope change of 1.32% from 0.3175 (the first image) to 0.3133 (the second image) was calculated, however the slope change was drastically different when the ligand was actually administered. In the case of the absence of ligand, the slope was measured to be 0.33554, compared to the presence of ligand, which the slope measured was 0.4824, yielding a 43.77% change in slope.

Once the cells were broken into sub-ranges of total concentration, there was an immediate difference at every level of expression but one, the 30 (29.999) - 40  $\mu\text{M}$  range (due to only one cell staying within the same concentration range in the absence to the presence of ligand as described in Chapter 2.7). Figure 4.9 depicts the various ranges of the sum total concentration of donors and acceptors, and the accompanying graphs of average  $E_{\text{app}}$  versus the molar concentration of acceptors, or  $X_A$ . The result appears to be that the ligand has a stronger effect on average  $E_{\text{app}}$  at higher sum of the total concentrations of donor and acceptors. The slope increases more and more as the concentrations increase. This may be the first time a measureable difference can be accounted for in the case of Ste2 in the absence and presence of the ligand.

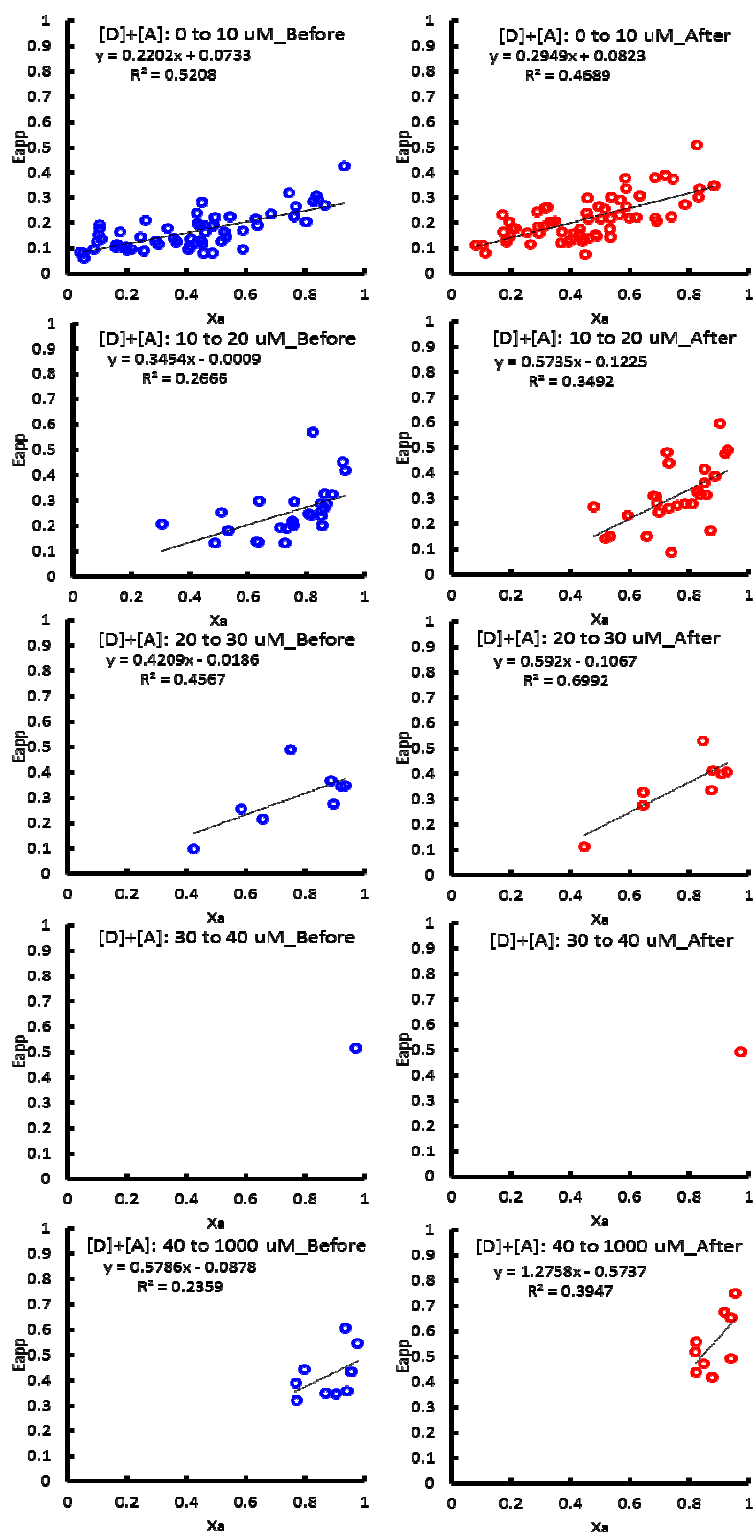


**Figure 4.9.** The plots of Average  $E_{app}$  versus Molar concentration of the acceptor ( $X_a$ ) for both the absence (labeled “Before”) and in the presence (labeled “After”) of the ligand. The points represent the same cells before and after introduction of the ligand. The slopes increase in all but one graph (due to slope being immeasurable).

This measured slope difference seen in Figure 4.9 may attributed to the ligand presence, but what it says about association is limited, in the absence of a detailed theoretical model. An increase in average FRET efficiencies may mean that the dimers are associating into tetramers and hence yield a higher overall efficiency, but this conclusion has to be validated through further experimentation and detailed theoretical modelling. We therefore conclude that these initial results show promise to indicate some effect of the ligand on the Ste2 protein, and it is likely that it is with regard to the association of the dimers into tetramers. Future research will have to take these studies and maximize the statistics and hopefully a more apparent structural analysis can come about.

## Chapter 5

### CONCLUSIONS AND FUTURE DIRECTIONS

The conclusions drawn from this research can be stated as follows: the lowest order stable oligomer found in Ste2 is the dimer and it is found in large numbers, but Ste2 also forms higher order oligomers, such as tetramers. The effect of the ligand is that there is a shift of proportions of dimers to tetramers after the introduction of the ligand. This does not mean that both species are not present after ligand, as it was found that they were. The experiment with averaging  $E_{app}$  vs  $X_A$  shows a larger shift at higher total (sum) concentrations of donors and acceptors. If a linear slope on the  $E_{app}$  vs.  $X_A$  graph shows the presence of dimers, then large deviations in the  $E_{app}$  axis must mean FRET efficiencies other than pairwise FRET efficiency, and if those deviations are vastly higher than the average, or linear slope, then that would also indicate the presence of tetramers because it is the only model to have peaks beyond  $E_p$ . This also confirms the results previously found by the Raicu group concerning the Ste2 receptor [22]. The meta-histogram shows promise to extract dimers if the dimers are present in the particular protein of interest. The question still remains if monomers are present, because neither of these experiments eluded to any detail regarding them. Monomers would add to the mixing of other oligomers and other peaks would begin to appear in the meta-histogram. If those mixtures did not present a high enough population to create a predominant peak, then they were not captured in the meta-histogram. So, only the mixtures of high enough population were fit, and it appears as though they were mostly dimers. Lastly, the meta-histogram may be washed out or broadly mixed by the tetramers or higher order oligomers mixing, but analyzing individual histograms yielded the result of a higher order oligomers, or in this case the tetramer.



Future models may be able to capture more than one complex per pixel for higher order oligomers, and hence researchers can look at higher expressing cells.

Knowing the concentration of donors and acceptors allowed for the calculation of the slopes of the plots of average  $E_{app}$  vs.  $X_A$ . The linear slope indicates that as the molar concentration of acceptors increases, so does the average  $E_{app}$ , which approached pairwise FRET efficiency, or  $E_d$ . This confirmed the findings from the meta-histogram that dimers are present. The spread beyond the trendline of the plots of average  $E_{app}$  vs.  $X_A$  also indicates there must be higher order oligomers present, because some cells exceeded the  $E_d$  value found in the meta-histogram, as discussed in Chapter 4.1.2. This agreement between the two separate experiments confirms that there are both oligomer sizes present within Ste2. The use of averaging provided insight to the effect that ligand may be having, which is that the ligand may help form tetramers from dimers to cooperatively release the G-protein in Ste2. The meta-histogram lacked this information, but did find the lowest order oligomer present, which may be inherent in meta-histograms in general. Meaning, that if dimers are present in a receptor, the meta-histogram will always emphasize them more compared to other oligomers due to the various combinations broadening it as discussed in Chapter 4.1.1.

Regarding future directions of the research, the consideration that the Ste2 used in these experiments lacked the ability to be internalized must be considered. As other researchers have found [13, 17], Ste2 internalizes due to ligand binding, and also release of the G-protein is considered an effect due to ligand signaling. What was not known was the effect of the ligand on the oligomeric size. This thesis emphasizes that the ligand does have an effect on oligomeric size, but that functionality might not be effected. To develop better insight, researchers would want to consider the use of cell trapping mechanisms, like microfluidic devices, that would allow for proper analysis of cells in the absence and presence of ligand. One

question that arose during the analysis was if the same voxel, or z-axis section was captured identically before and after introduction of the ligand. A microfluidic device would allow for a more accurate measurement in all dimensions since the cell is fully immobilized. This is one of two avenues of future research that can be considered experimentally.

The next experimental avenue of future research might be to look at internalization of the Ste2 receptor. As stated above, the Ste2 used in these experiments has been genetically modified to not internalize. The use of the wild-type Ste2 would allow for the exploration into Ste2 internalization and G-protein release. By using the above mentioned microfluidic device, and a fluorescently tagged ligand as well as a tagged G-protein, one could theoretically watch the entire sequence of the Ste2 internalization and G-protein release by using different species of fluorescent tags and properly spectrally unmixing each. This would be a true revelation in the field of GPCR signaling and the G-protein second messenger system. Likewise, researchers could explore recycling of the Ste2 receptor, as well as looking into if the ligand breaches the cellular membrane without binding to Ste2.

The final note to future researchers may be that the effect due to something called stochastic FRET is unknown at the present [50, 51]. The stochastic FRET is an undesired energy transfer due to physical interaction, but low amounts of physical interaction occur between these receptors in other cases [51]. It is known to exist, but not its extent, however thus far has been considered negligible at lower concentrations. What is known is that the higher the expression level, the higher the stochastic FRET becomes, and hence higher FRET efficiencies. This may play a role in measuring quaternary structure of receptors using FRET and future research will be needed to extract this stochastic FRET and separate it from functional FRET.

## REFERENCES

1. Kresge, N., Simoni, R.D., Hill, R.L., *Earl W. Sutherland's discovery of cyclic adenine monophosphate and the second messenger system*. Biochemical Journal. **232**. 1077-1092 (1958).
2. *The Martin Rodbell Papers: Signal Transduction and the discovery of G-proteins, 1969-1980*. National Institute of Health. Last accessed November 19, 2014. Retrieved from <http://www.profiles.nlm.nih.gov/ps/retrieve/Narrative/GG/p-nid/41>
3. Dixon, R.A.F., Kobilka, B.K., Leftkowitz, R.J., Strader, C.D., et al., *Cloning of the gene and cDNA for mammalian  $\beta$ -adrenergic receptor and homology with rhodopsin*. Nature. **321**. 75-79 (1986).
4. Rasmussen, S.G.F., Kobilka, B.K., et al., *Crystal structure of the human  $\beta_2$  adrenergic G-protein-coupled receptor*. Nature. **450**. 383-387 (2007).
5. Rosenbaum, D.M., Kobilka, B.K., et al., *GPCR engineering yields high-resolution structural insights into  $\beta_2$ -adrenergic receptor function*. Science. **318(5854)**. 1266-1273 (2007).
6. Rasmussen, S.G.F., Kobilka, B.K., et al., *Crystal Structure of the  $\beta_2$  adrenergic receptor-Gs protein complex*. Nature. **477**. 549-555 (2011).
7. Filmore, D., *It's a GPCR World*. Modern Drug Discovery (American Chemical Society). November Edition. 24-28 (2004).
8. Overington, J.P., Al-Lazikani, B., Hopkins, A.L., *How many drug targets are there?* National Rev. Drug Discovery. **5(12)**. 993-996 (2006).
9. Schmidt, M., Saldin, D.K., *Enzyme transient state kinetics in crystal and solution from the perspective of a time-resolved crystallographer*. Structural Dynamics **1**. 024701 (2014).
10. Schmidt, M., Nienhaus, K., Pahl, R., Krasselt, A., Nienhaus, U., Parak, F., Srajer, V., *Ligand migration pathway and protein dynamics in myoglobin: A time-resolved crystallographic study on L29W MbCO*. Proc. Natl. Acad. Sci. USA **13**. 11704-11709 (2005).
11. Sartori, A., Gatz, R., Beck, F., Rigort, A., Baumeister, W. and Plitzko, J. M., *Correlative microscopy: bridging the gap between fluorescence light microscopy and cryo-electron tomography*. Journal of Structural Biology. **160**. 135-145 (2007).
12. Sprague, B.L., Pego, R.L., Stavreva, D.A., McNally, J.G., *Analysis of binding reactions by fluorescence recovery after photo bleaching*. Biophysical Journal. **86(6)**. 3473-3495 (2004).
13. Yesilaltay, A., Jenness, D.D., *Homo-oligomeric complexes of the yeast  $\alpha$ -factor pheromone receptor are functional units of endocytosis*. Molecular Biology of the Cell. **11**. 2873-2884 (2000)
14. Nakayama, N., Miyajima, A., Arai, K., *Nucleotide sequences of STE2 and STE3, cell type-specific sterile genes from Saccharomyces cerevisiae*. EMBO J. **10**. 2643-2648 (1985).
15. Burkholder, A.C., Hartwell, L.H., *The yeast alpha-factor receptor: structural properties deduced from the sequence of the STE2 gene*. Nucleic Acid Res. **13(23)**. 8463-8475 (1985).
16. Herskowitz, I., Marsh, L., *STE2 protein of Saccharomyces kluyveri is a member of the rhodopsin/beta-adrenergic receptor family and is responsible for the recognition of the peptide ligand alpha factor*. Pro. Natl. Acad. Sci. U.S.A. **85(11)**. 3855-3859 (1988).
17. Overton, M.C, Chinault, S.L., Blumer, K.J., *Minireview: Oligomerization of G-protein-coupled receptors: lessons from the yeast Saccharomyces cerevisiae*. Eukaryotic Cell. **4(12)**. 1963-1970 (2005).
18. Milligan, G., *The Prevalence, Maintenance, and Relevance of G Protein-Coupled Receptor Oligomerization*. Molecular Pharmacology. **84(1)**: p. 158-169 (2013).

19. Granier, S. and B. Kobilka, *A new era of GPCR structural and chemical biology*. Nature Chemical Biology. **8**(8): p. 670-673(2012).
20. Palczewski, K., *Oligomeric forms of G protein-coupled receptors (GPCRs)*. Trends in Biochemical Sciences. **35**(11): p. 595-600(2010).
21. Park, P.S.-H. and J.W. Wells, *Monomers and oligomers of the M2 muscarinic cholinergic receptor purified from Sf9 cells*. Biochemistry. **42**(44): p. 12960-12971(2003).
22. Raicu, V., et al., *Determination of supramolecular structure and spatial distribution of protein complexes in living cells*. Nat. Photonics. **3**: p. 107-113(2009).
23. Parnot, C. and B. Kobilka, *Toward understanding GPCR dimers*. Nature Structural & Molecular Biology. **11**(8): p. 691-692(2004).
24. Overton, M.C., S.L. Chinault, and K.J. Blumer, *Oligomerization of G-protein-coupled receptors: lessons from the yeast Saccharomyces cerevisiae*. Eukaryot. Cell. **4**(12): p. 1963-70(2005).
25. Ma, A.W., A.B. Pawagi, and J.W. Wells, *Heterooligomers of the muscarinic receptor and G proteins purified from porcine atria*. Biochem. Biophys. Res. Communications. **374**(1): p. 128-33(2008).
26. Chabre, M. and M. le Maire, *Monomeric G-protein-coupled receptor as a functional unit*. Biochemistry. **44**(27): p. 9395-403(2005).
27. Gurevich, V.V. and E.V. Gurevich, *Rich tapestry of G protein-coupled receptor signaling and regulatory mechanisms*. Mol Pharmacol. **74**(2): p. 312-6(2008).
28. Hern, J.A., et al., *Formation and dissociation of M-1 muscarinic receptor dimers seen by total internal reflection fluorescence imaging of single molecules*. Proceedings of the National Academy of Sciences of the United States of America. **107**(6): p. 2693-2698(2010).
29. Calizo, R.C., Scarlata, S., *Discrepancy between fluorescence correlation spectroscopy and fluorescence recovery after photobleaching diffusion measurements of G-protein-coupled receptors*. Analytical Biochemistry. **440**(1). 40-48 (2013).
30. Herrick-Davis, K., Grinde, E., Cowan, A., Mazurkiewicz, J.E., *Fluorescence Correlation Spectroscopy Analysis of Serotonin, Adrenergic, Muscarinic, and Dopamine Receptor Dimerization: The Oligomer Number Puzzle*. Molecular Pharmacology. **84**(4). 630-642 (2013).
31. Barbeau, A., Godin, A.G., Swift, J.L., De Konnick, Y., Wiseman, P.W., Beaulieu, J.M., *Quantification of Receptor Tyrosine Kinase Activation and Transactivation by G-Protein-Coupled Receptors Using Spatial Intensity Distribution Analysis (SpiDA)*. G Protein Coupled Receptors: Modeling, Activation, Interactions and Virtual Screening. **522**. 109-131 (2013).
32. Sergeev, M., Godin, A.C., Kao, L., Abuladze, N., Wiseman, P.W., Kurtz, I., *Determination of Membrane Protein Transporter Oligomerization in Native Tissue Using Spatial Fluorescence Intensity Fluctuation analysis*. PLOS One. **7**(4). e36215 (2012).
33. Singh, D.R., Mohammad, M.M., Patowary, S., Stoneman, M.R., Oliver, J.A., Movileanu, L., Raicu, V., *Determination of the quaternary structure of a bacterial ATP-binding cassette (ABC) transporter in living cells*. Integrative Biology. **5**(2). 312-323 (2013).
34. Raicu, V., *FRET-based determination of protein complex structure at nanometer length scale in living cells*. In Nanoscopy and Multidimensional Optical Fluorescence Microscopy (Diaspro A., ed.), CRC press, Boca Raton.
35. Patowary, S., Alvarez-Curto, E., Xu, T.R., Holz, J.D., Oliver, J.A., Milligan, G., Raicu, V., *The muscarinic M3 acetylcholine receptor exists as two differently sized complexes at the plasma membrane*. Biochemical Journal. **452**(2). 301-312 (2013).

36. Yuan, L., Lin, W.Y., Zheng, K.B., Zhu, S.S., *FRET-Based Small-Molecule Fluorescent Probes: Rational Design and Bioimaging Applications*. Accounts of Chemical Research. **46(7)**. 1462-1473 (2013).
37. Raicu, V., Jansma, D.B., Miller, R.J.D., Friesen, J.D., *Protein interaction quantified in vivo by spectrally resolved fluorescence resonance energy transfer*. Biochemical Journal. **385**. 265-277 (2005).
38. Stoneman, M.R., Singh, D.R., Raicu, V., *In vivo quantification of G protein coupled receptor interactions using two-photon microscopy*. Journal of Visualized Experiments. **47:e2247** (2011).
39. Gehret, A.U., Connelly, S.M., Dumont, M.E., *Functional and Physical Interactions among Saccharomyces cerevisiae alpha-Factor Receptors*. Eukaryotic Cell. **11(10)**. 1276-1288 (2012).
40. Raicu, V. and D.R. Singh, *FRET Spectrometry: A New Tool for the Determination of Protein Quaternary Structure in Living Cells*. Biophysical Journal **105(9)**: p. 1937-1945. (2013).
41. Zimmerman, T., Rietdorf, J., Girod, A., Georget, V., Pepperkok, R., *Spectral imaging and linear un-mixing enables improved FRET efficiency with a novel GFP2-YFP FRET pair*. FEBS Lett. **531(2)**. 245-249 (2002).
42. Lippincott-Schwartz, J., Patterson, G.H., *Development and use of fluorescent protein markers in living cells*. Science. **300(5616)**. 87-91 (2003).
43. Stefan, C.J., Blumer, K.J., *A syntaxin homolog encoded by VAM3 mediates down-regulation of a yeast G protein-coupled receptor*. Journal of Biological Chemistry. **274(3)**. 1835-1841 (1999)
44. Asawa, H., Hiruoka, Y., Haragachi, T., *Live CLEM imaging: an application for yeast cells*. Formatex Research Center. 2012.
45. Sandin, R.L., *Studies on cell adhesion and Concanavalin A agglutination of Candida albicans after mannan extraction*. Journal of Medical Microbiology. **24**. 145-150 (1987).
46. Biener, G., et al., *Development and Experimental Testing of an Optical Micro-Spectroscopic Technique Incorporating True Line-Scan Excitation*. International Journal of Molecular Sciences. **15(1)**: p. 261-276 (2014).
47. Stoneman, M.R., Patowary, S., Singh, D.R., Komarova, L., Westrick, L.G., Oliver, J.A., Raicu, V., *Quantifying the efficiency of various FRET constructs using OptiMiS™*. BioTechniques. **52(3)**. 191-195 (2012).
48. Raicu, V., *Nanoscopy and Multidimensional Optical Fluorescence Microscopy*. Chapman and Hall. Edited by Alberto Diaspro. Pages 13-1:13-8 (2010).
49. Lee, N.K. et al. *Three color alternating-laser excitation of single molecule monitoring multiple interactions and distances*. Biophysical Journal. **92(1)**. (2007).
50. Wolber, P.K., Hudson, B.S., *An analytical solution to the Forster energy transfer problem in two dimensions*. Biophys. J. **28**. 197-210 (1979).
51. Singh, D.R., Raicu, V., *Comparison between Whole Distribution- and Average-Based Approaches to the Determination of Fluorescence Resonance Energy Transfer Efficiency in Ensembles of Proteins in Living Cells*. Biophys. J. **98**. 2127-2135 (2010).